FINAL TECHNICAL REPORT

Research Grant: DE-FG02-08ER54951

Recipient: Board of Regents, NSHE, obo University of Nevada, Reno

Project title: Theoretical Study of Radiation from a Broad Range of Impurity Ions for Magnetic Fusion Diagnostics

Principal Investigator: Prof. Alla Safronova

Start date of the grant: December 15, 2007
End date of the grant: December 14, 2013

Date of the report: March 14, 2014

Contents

Abtstract

Spectroscopy of radiation emitted by impurities plays an important role in the study of magnetically confined fusion plasmas. The measurements of these impurities are crucial for the control of the general machine conditions, for the monitoring of the impurity levels, and for the detection of various possible fault conditions. Low-Z impurities, typically present in concentrations of 1%, are lithium, beryllium, boron, carbon, and oxygen. Some of the common medium-Z impurities are metals such as iron, nickel, and copper, and high-Z impurities, such as tungsten, are present in smaller concentrations of 0.1% or less. Despite the relatively small concentration numbers, the aforementioned impurities might make a substantial contribution to radiated power, and also influence both plasma conditions and instruments. A detailed theoretical study of line radiation from impurities that covers a very broad spectral range from less than 1 Å to more than 1000 Å has been accomplished and the results were applied to the LLNL Electron Beam Ion Trap (EBIT) and the Sustained Spheromak Physics Experiment (SSPX) and to the National Spherical Torus Experiment (NSTX) at Princeton. Though low- and medium-Z impurities were also studied, the main emphasis was made on the comprehensive theoretical study of radiation from tungsten using different state-of-the-art atomic structure codes such as Relativistic Many-Body Perturbation Theory (RMBPT). The important component of this research was a comparison of the results from the RMBPT code with other codes such as the Multiconfigurational Hartree–Fock developed by Cowan (COWAN code) and the Multiconfiguration Relativistic Hebrew University Lawrence Atomic Code (HULLAC code), and estimation of accuracy of calculations. We also have studied dielectronic recombination, an important recombination process for fusion plasma, for variety of highly and low charged tungsten ions using COWAN and HULLAC codes. Accurate DR rate coefficients are needed for describing the ionization balance of plasmas, which in turn determines the lines contributing to the spectral emission and the radiative power loss. In particular, we have calculated relativistic atomic data and corresponding dielectronic satellite spectra of highly ionized W ions, such as, for example, Li-like W (with the shortest wavelength of x-ray radiation of about 0.2 Å) that might exist in ITER core plasmas at very high temperatures of 30-40 keV. In addition, we have completed relativistic calculations of low ionized W ions from Lu-like (W^{3+}) to Er-like (W^{6+}) and for Sm-like(W^{12+}) and Pm-like (W^{13+}) that cover a spectral range from few hundred to thousand Å and are more relevant to the edge plasma diagnostics in tokamak.

1. **Motivation and Summary of Results**

The main results of the project are highligted in the papers [1-23], PhD dissertations [24-25], and were presented at 39th, 40th 41st, 42nd, 43rd and 44th Annual Meetings of the APS Division of Atomic, Molecular, and Optical Physics, 17th, 18th, and 19th Topical Conference on High Temperature Plasma Diagnostics, 35th and 36th IEEE International Conferences on Plasma Science, 16th International Conference on Atomic Processes in Plasmas, and at 50th and 51st Annual Meetings of the Division of Plasma Physics as well as at other Intrenational Conferences and Workshops [26-57]. What was a motivation for this project?

Spectroscopy of radiation emitted by impurities plays an important role in the study of magnetically confined fusion plasmas (see, for example, [58]). The measurements of these impurities will be important for the control of the general machine conditions, for the monitoring of the impurity levels, and for the detection of various possible fault conditions. Low-Z impurities, typically present in concentrations of 1%, are lithium, beryllium, boron, carbon, and oxygen. Some of the common medium-Z impurities are metals such as iron, nickel, and copper and high-Z impurities such as tungsten are present in smaller concentrations of 0.1% or less. Despite the relatively small concentration numbers, the aforementioned impurities may have substantial contribution in radiated power and influence both plasma conditions and instruments. It is very important to study tungsten (W, z=74) radiation for development of reliable diagnostics of the impurities for the International Thermo-Nuclear Experimental Reactor (ITER). ITER represents the essential next step in a magnetic fusion and is the world's biggest fusion energy research project [59]. The expected main plasma impurities are beryllium and copper originating from the surface of the first wall in the main chamber, and carbon and tungsten from the divertor. All the main plasma regions of ITER will be probed by an extensive set of spectroscopic diagnostics covering the broadest from visible to x-ray wavelength range. The expected plasma parameters will also vary in a broad range. For example, the central electron/ion temperatures will be up to ~20-40 keV and the electron density will be up to ~10^{20} m^{-3}. Also, in the divertor it is predicted that the density will be one order higher but the temperature will be lower, from 1 to 100 eV, to reduce the heat flux on the divertor plate by increasing radiation power [59]. In 2008, Peter Beiersdorfer from LLNL and his co-workers installed several high-resolution spectrometers on the National Spherical Torus Experiment (NSTX), such as X-ray and Extreme Ultraviolet spectrometer XEUS [60], which has a ~50Å field of view that can be positioned to cover a spectral region from 5 to 135 Å and a collection of high-resolution data that include most of

mentioned impurities was recorded on NSTX. Together with some data from the Sustained Spheromak Physics Experiment (SSPX). NSTX data became available for comprehensive spectroscopic studies and modeling of impurities. Though low- and medium-Z impurities were also studied, the main emphasis was made on the comprehensive theoretical study of radiation from tungsten using different state-of-the-art atomic structure codes such as Relativistic Many-Body Perturbation Theory (RMBPT) code (see, for example, [1]). The important component of this research was a comparison of the results from the RMBPT code with other codes such as the Multiconfigurational Hartree–Fock developed by Cowan (COWAN code) [61] and the Multiconfiguration relativistic Hebrew University Lawrence Atomic Code (HULLAC code) [62]. We also have studied dielectronic recombination for variety of very highly charged tungsten ions using COWAN and HULLAC codes. Dielectronic recombination (DR) is an important recombination process for tokamak plasmas. Non-Local Thermodynamic Equilibrium (non-LTE) modeling of EUV/X-ray spectra were based on the atomic data calculated using Flexible Atomic Code [63].

2. Relativistic calculations of W ions and work relevant to study of W radiation

The tungsten plasma produced under very different temperatures from tens eV up to the highest values of 40 keV represent a very important object of present theoretical and future experimental research. This part of our work was focused on the comprehensive theoretical study of radiation from tungsten and development of relativistic atomic data using different state-of-the-art atomic structure codes. It also includes non-LTE modeling of spectra and identification of spectral features important for diagnostics of high-temperature tungsten plasmas. The details of this study are given below.

2.1 Excitation energies, radiative and autoionization rates, dielectronic satellite lines, and dielectronic recombination rates for excited states for *highly ionized W*

The most abundant W ions in the 7–40 keV range are highly ionized S-like (W^{58+}) to Li-like (W^{71+}) ions (see, for example, [64]). The list of highly ionized tungsten ions studied in this project along with references to the published papers and a PhD dissertation is presented in Table 1 below. First, we consider the summary of theoretical results for highly ionized tungsten ions which include excitation energies, radiative and autoionization rates, dielectronic satellite lines, and dielectronic recombination rates for excited states of Na-, Mg- and Li-like W.

a) Ni-like ions with focus on Ni-like W [1, 2, 14]

Transition rates and line strengths were calculated for electric-multipole ($E2$ and $E3$) and magnetic-multipole ($M1$, $M2$, and $M3$) transitions between $3s^2 3p^6 3d^{10}$, $3s^2 3p^6 3d^9 4l$, $3s^2 3p^5 3d^{10} 4l$, and $3s 3p^6 3d^{10} 4l$ states (with $4l$=$4s$, $4p$, $4d$, and $4f$) in Ni-like ions with the nuclear charges ranging from Z=34 to 100. Relativistic many-body perturbation theory (RMBPT), including the Breit interaction, is used to evaluate retarded multipole matrix elements. Transition energies used in the calculation of line strengths and transition rates are from second-order RMBPT. Lifetimes of the $3s^2 3p^6 3d^9 4s$ levels are given for Z=34–100. Taking into account that calculations were performed in a very broad range of Z, most of the data are presented in graphs as Z dependences. The full set of data is given only for Ni-like W ion. In addition, we also give complete results for the $3d4s\ ^3D_2$–$3d4s\ ^3D_1$ magnetic-dipole transition, as the transition may be observed in future experiments, which measure both transition energies and radiative rates. These atomic data are important in the modeling of radiation spectra from Ni-like multiply charged ions generated in electron beam ion trap experiments as well as for laboratory plasma diagnostics including fusion research.

Table 1. List of the tungsten ions studied in the project including their ground states, ionization potentials, references to the published papers, and comments.

Ion	Ground State	IP(eV) [10]	References this work	Comments
Ag-like W (W^{27+})	[Ni]$4s^2 4p^6 4d^{10} 4f$	881.4	[6]	theory
Ge-like W (W^{42+})	[Ni]$4s^2 4p^2$	2149.2	[2, 14]	exp and theory
Ga-like W (W^{43+})	[Ni]$4s^2 4p$	2210.0	[2, 14]	exp and theory
Zn-like W (W^{44+})	[Ni]$4s^2$	2354.5	[2, 7, 14]	exp and theory
Cu-like W (W^{45+})	[Ni]4s	2414.11	[2, 14, 17]	exp and theory
Ni-like W (W^{46+})	[Ni]	4057	[1, 2, 14]	exp and theory
Co-like W (W^{47+})	[Ne]$3s^2 3p^6 3d^9$	4180	[2, 14]	exp and theory
Ca-like W (W^{54+})	[Ne]$3s^2 3p^6 3d^3$	5209	[7]	theory
Al-like W (W^{61+})	[Ne]$3s^2 3p$	6735	[7]	theory
Mg-like W (W^{62+})	[Ne]$3s^2$	7000	[5, 7]	theory
Na-like W (W^{63+})	[Ne]3s	7130	[4]	theory
Ne-like W (W^{64+})	[Ne]	15566	[4]	theory
B-like W (W^{69+})	[He]$2s^2 2p$	18872	[7]	theory
Be-like W(W^{70+})	[He]$2s^2$	19362	[7]	theory
Li-like W (W^{71+})	[He]2s	19691	[8]	theory

b) <u>Na-like W from Ne-like W [4]</u>

Tungsten will become near Ne-like in the core of the plasma produced by ITER, which allows the use of L-shell tungsten spectra as a core diagnostic. Na-like dielectronic satellites of Ne-like tungsten will thus likely play an important role in L-shell x-ray diagnostic for future magnetic fusion plasmas, and accurate atomic data will be needed to assess line broadening, shifts of line centroids, and the charge balance. With this in mind, we have made the comprehensive calculations of Na-like tungsten dielectronic recombination (DR) atomic data. Energy levels, radiative transition probabilities, and autoionization rates for $1s^22s^22p^53l'nl$, $1s^22s2p^63l'nl$ (n = 3-7, $l \leq n$-1) and $1s^22s^22p^54l'nl$, $1s^22s2p^64l'nl$ (n = 4-6, $l \leq n$- 1) states in Na-like tungsten (W^{63+}) are calculated by the Cowan code, the HULLAC code and using the relativistic many-body perturbation theory method by the RMBPT code. Autoionizing levels above the threshold $1s^22s^22p^6$ are considered. It is found that configuration mixing [$3snp + 3pns + 3pnd + 3dnp$], [$3sns + 3pnp + 3dnd$] plays an important role for all atomic characteristics. Also the strong mixing between states with $2s$ and $2p$ holes ($1s^22s^22p^53l_1nl_2 + 1s^22s2p^63l_3nl_4$) occurs. Branching ratios relative to the first threshold and intensity factors are calculated for satellite lines, and dielectronic recombination (DR) rate coefficients are determined for the excited $1s^22s^22p^6nl$ (n = 3-7, $l \leq n$ - 1) states. It is shown that the contribution of the highly-excited states is very important for calculation of total DR rates. Contributions from the autoionization states $1s^22s^22p^53l'nl$, $1s^22s2p^63l'nl$ ($n \geq 8$) and $1s^22s^22p^54l'nl$, $1s^22s2p^64l'nl$ ($n \geq 7$) to DR rate coefficients are estimated by extrapolation of all atomic parameters. The orbital angular momentum quantum number l distribution of the rate coefficients shows a peak at l=2. The total DR rate coefficient is derived as a function of electron temperature. Synthetic spectra were constructed of dielectronic satellite lines for transitions ($2s^22p^63l$ - $2s^22p^53lnl'$ and $2s^22p^63l$ - $2s2p^63lnl'$) at Te = 2 keV in a spectral region 0.77 - 1.6 Å and for ($2s^22p^64l$ - $2s^22p^54lnl'$ and $2s^22p^64l$ - $2s2p^64lnl'$) at Te = 2 keV and 10 keV in a spectral region 0.78 - 1.05 Å.

c) <u>Mg-like W from Na-like W [5, 7]</u>

We calculated a large set of atomic data relevant to the dielectronic recombination of Na-like W into Mg-like W^{62+}. Energy levels, radiative transition probabilities and autoionization rates for $1s^22s^22p^63l'nl$ (n = 3–13, $l \leq n - 1$), $1s^22s^22p^64l'nl$ (n = 4–7, $l \leq n - 1$) and $1s^22s^22p^53l'3l''nl$ (n = 3–4, $l \leq n - 1$) states in Mg-like tungsten (W^{62+}) are calculated using COWAN code, the HULLAC code and the relativistic many-body perturbation theory

method by the RMBPT code. Autoionizing levels above the thresholds $1s^2 2s^2 2p^6 3l$ and $1s^2 2s^2 2p^6 4l$ are considered. Branching ratios relative to the first threshold and intensity factors are calculated for satellite lines, and dielectronic recombination (DR) rate coefficients are determined for the first excited odd- and even-parity states. It is shown that the contribution of the highly excited states is very important for the calculation of total DR rates. Contributions to DR rate coefficients from the excited $1s^2 2s^2 2p^6 3l'nl$ states with $n \geq 14$ and $1s^2 2s^2 2p^6 4l'nl$ states with $n \geq 8$ and additionally from core-excited $1s^2 2s^2 2p^5 3l'3l''nl$ states with $n \geq 5$ are estimated by extrapolation of all atomic parameters. The orbital angular momentum quantum number l distribution of the rate coefficients shows two peaks at $l = 2$ and $l = 5$. The total DR rate coefficient is derived as a function of electron temperature. Most of the state-selective DR rate coefficients reveal a double peak as a function of electron temperature. The transitions through intermediate states $2p^6 3l'nl$, $2p^6 4l'nl$ and $2p53l'3l''nl$ produce a peak in the DR rate coefficients at *Te* at about 50 eV, 70 eV and 2.1 keV, respectively. The state-selective rate coefficients can be used in collisional-radiative models aimed at investigating the population kinetics in recombining plasmas as well as in calculation of ionization equilibrium.

Another important results of the paper are L-shell dielectronic satellite spectra of W. Figure 1 shows examples of DS spectra for *Te* = 10 keV generated by the $2p^6 3lnl'–2p^5 3l_1 3l_2 n_3 l_3$ transitions. In this figure, we include data for 1032 even-odd parity transitions and 862 odd-even parity transitions. The effective emission rate coefficients $C^{\text{eff}}(j, i)$ and Gaussian profiles with spectral resolution $R \equiv \lambda/\Delta\lambda = 2000$ are used to synthesize these spectra. The limited set of the transitions includes transitions with $320 > C^{\text{eff}}(j, i) > 0.1$ in units of 10^{-15} $\text{cm}^3\ \text{s}^{-1}$. The synthetic spectrum of DS lines from the W^{62+} ion at *Te* = 10 keV is divided into four spectral regions: λ=0.94–1.09 Å, λ=1.17–1.25 Å, λ=1.28–1.38 Å and λ = 1.38–1.59 Å.

The strongest lines shown in Fig. 1a are due to the $2p^6 3s3p–2p^5 3s3p3d$, $2p^6 3s3d–2p^5 3s3d^2$ and $2p^6 3p^2–2p^5 3s3p^2$ transitions in the very narrow region of λ = 1.2026–1.2031 Å with C^{eff} equal to 34–119 in units of 10^{-15} $\text{cm}^3\ \text{s}^{-1}$. Those lines are the satellite lines to the $2p_{1/2}– 3d_{3/2}$ resonance line at λ = 1.2019 Å of Ne-like tungsten [4]. We note one other strong line with C^{eff} equal to 45.5 in units of 10^{-15} $\text{cm}^3\ \text{s}^{-1}$. It is identified as the $2p^6 3s^2–2p^5 3s3p^2$ transition. This line is caused by the mixing of the $2p^5 3s3p^2$ states with the $2p^5 3s^2 3d$ states. The strongest lines shown in Fig. 1b are due to the $2p^6 3s3p–2p^5 3s3p3d$, $2p^6 3s3d–2p^5 3s3d^2$ and $2p^6 3p^2–2p^5 3s3p^2$ transitions. They are displayed in the very narrow spectral region of λ = 1.3755–1.3762 Å with C^{eff} equal to 20–85 in units of 10^{-15} $\text{cm}^3\ \text{s}^{-1}$. Those lines should be the

satellite lines to the $2p_{3/2}$–$3d_{3/2}$ resonance lines at λ =1.3786 Å of Ne-like tungsten. The satellite lines to the 2p–3s transition in Ne-like tungsten (at λ=1.4927 Å) are displayed in Fig. 1c. The strongest satellite lines are due to the $2p^6 3s3p$– $2p^5 3s^2 3p$, $2p^6 3p^2$–$2p^5 3s3p^2$ and $2p^6 3p3d$–$2p^5 3s3p3d$ transitions in the spectral region of λ = 1.5080–1.5145 Å with C^{eff} equal to 5–30 in units of 10^{-15} $\text{cm}^3\,\text{s}^{-1}$. The satellite lines to the 2p–4d transition in Ne-like tungsten (at λ = 1.0416 Å) are displayed in Fig. 1d. The strongest satellite lines are due to the $2p^6 3s3p$–$2p^5 3s3p4d$ and $2p^6 3s3d$–$2p^5 3s3d4d$ transitions in the very narrow spectral region of λ = 1.0552–1.0563 Å with C^{eff} equal to 5–20 in units of 10^{-15} $\text{cm}^3\,\text{s}^{-1}$. The dielectronic satellite spectra of W^{62+} are important for L-shell diagnostic of very high-temperature laboratory plasmas such as future ITER plasmas.

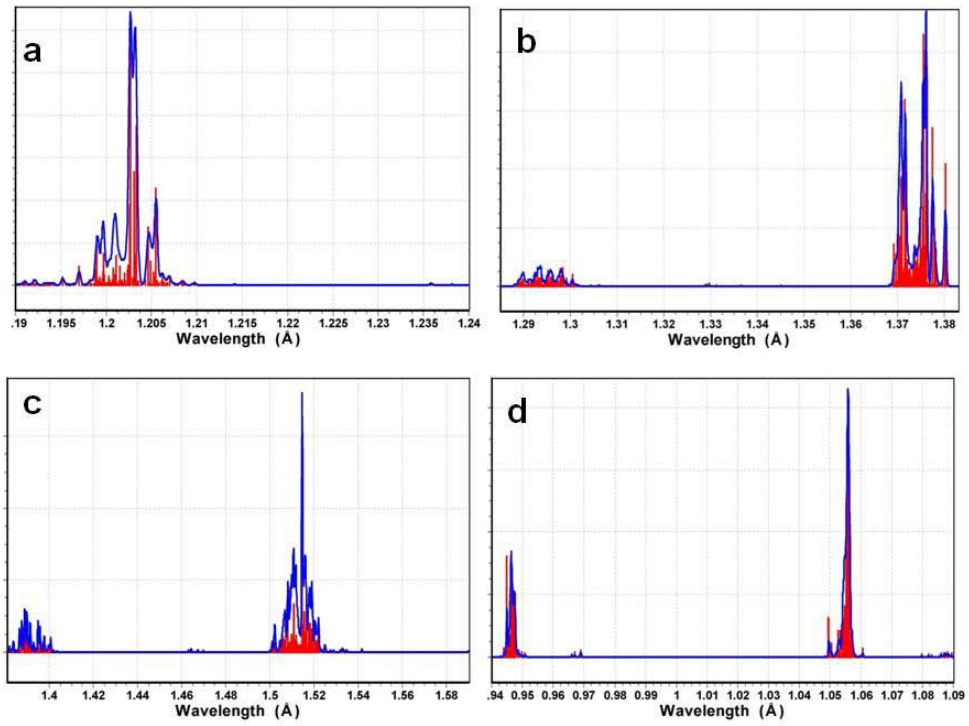

Fig. 1. Dielectronic satellites to the Ne-like resonance lines $2p_{1/2}3d_{3/2}$ at 1.2019 Å (a), $2p_{3/2}3d_{3/2}$ at 1.3786 Å (b), $2p_{3/2}3s_{1/2}$ at 1.4927 Å (c), and $2p_{3/2}4d_{3/2}$ at 1.0416 Å (d) [5].

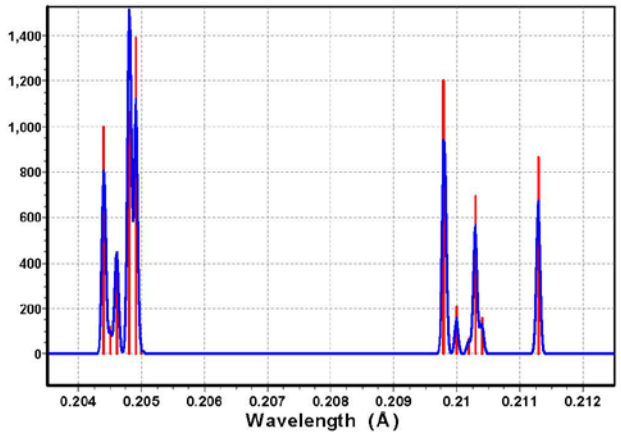

Fig. 2. Synthetic spectra (red) of dielectronic satellite lines (2l2l'1s - $1s^2$2l'') from the W^{71+} ion at Te = 40 keV for λ= 0.204 - 0.212 Å. A resolving power, R = λ/Δλ = 3000 is assumed to produce a Gaussian profile (blue). The scale in the ordinate is in units of 10^{-13} cm^3/s [8].

d) Li-like ions from He-like ions (with focus on W ions) [8]

Energy levels, radiative transition probabilities, and autoionization rates are calculated for 1s2l2l' states in lithiumlike ions with nuclear charges ranging from Z = 6 to 100. Relativistic many-body perturbation theory (RMBPT), including the Breit interaction, is used to evaluate atomic properties. Second-order RMBPT is used to determine energy levels and radiative matrix elements. Non-radiative matrix elements are calculated in first-order RMBPT. First-order perturbation theory is used to obtain intermediate coupling coefficients which are, in turn, used to evaluate energies, radiative, and non-radiative rates. These data are used to obtain branching ratios, intensities, and effective emission rate coefficients of dielectronic satellite lines. Trends of relative intensity factors as functions of nuclear charge Z are shown graphically for the 1s2l'2l'' - $1s^2$2l transitions. Though the RMBPT data were calculated for the broad range of nuclear charges Z from 6 to 100, the main emphasis as well as a detailed discussion of correlation contributions to evaluated characteristics were made for lithiumlike tungsten, Z = 74. Synthetic spectra of dielectronic satellite lines (2l2l'1s - $1s^2$2l'') from the Mo^{39+} (Te = 7.5 keV) and W^{71+} ion (Te = 40 keV) ions are constructed using the complete set of RMBPT data. Fig. 2 shows an example of synthetic dielectronic satellite spectra for Li-like W ions generated by the 1s2l2l'- 1s22l'' transitions. The effective emission rate coefficients C^{eff} (j; i) and Gaussian profiles with spectral resolution $R = \lambda/\Delta\lambda$ = 3000-5000 are used to synthesize these spectra. In particular, Li-like spectra cover the spectral range from 0.687 - 0.701 Å for Mo and from 0.204 to 0.212 Å for W ions. The most prominent dielectronic satellite lines are due to $1s2p^2\ ^2D_{5/2}$ - $1s^22p\ ^2P_{3/2}$, $1s2p^2\ ^2D_{3/2}$ - $1s^22p\ ^2P_{1/2}$, and $1s2s2p\ ^2P_{1/2,3/2}$ - $1s^22s\ ^2S_{1/2}$ transitions. These results are relevant to spectroscopic diagnostics of plasmas of a broad range of parameters and up to very highest temperature plasmas such as future ITER plasmas.

e) Wavelengths and transition rates for nl − n'l' transitions in Be-, B-, Mg-, Al-, Ca-, Zn-, Ag-, and Yb-like tungsten ions [7]

We accomplished a comprehensive theoretical study of atomic characteristics of eight isoelectronic sequences of tungsten ions in a broad range of wavelengths and transitions. In particular, excitation energies, oscillator strengths, and transition probabilities are calculated for $nl - n'l'$ transitions in W^{70+}, W^{69+}, W^{62+}, W^{61+}, W^{54+}, W^{44+}, W^{27+} and W^{4+} ions. Atomic structure and radiative characteristics of Be-like ([He]2*lnl'*, *n* = 2, 3), B-like ([He]2*l*2*l'*2*l''*), Mg-like ([Ne]3*l*3*l'*), Al-like ([Ne]3*l*3*l'*3*l''*), Ca-like ([Ar]3*d*4*l*), Zn-like ([Ni]4*l*4*l'*), Ag-like [Kr]$4d^{10}nl$), and Yb-like ([Xe]$4f^{14}$5*l*6*l'*) tungsten ions are computed by relativistic many-body

perturbation theory (RMBPT) method. The calculations start from a $1s^2$ Dirac-Fock potential for Be- and B-like W, from the $1s^22s^22p^6$ Dirac-Fock potential for Mg- and Al-like W; from the $1s^22s^22p^63s^23p^6$ and $1s^22s^22p^63s^23p^63d^{10}$ Dirac-Fock potentials for Ca- and Zn-like W, respectively. Evaluation of properties of Ag-like and Yb-like ions starts from a Dirac-Fock potential with only partially filled $n = 4$ shell ($1s^22s^22p^63s^23p^63d^{10}4s^24p^64d^{10}$) and $n = 5$ shell ($1s^22s^22p^63s^23p^63d^{10}4s^24p^64d^{10}4f^{14}5s^25p^6$), respectively. First-order perturbation theory is used to obtain intermediate coupling coefficients, and the second-order RMBPT is used to determine the matrix elements. The contributions from negative-energy states are included in the second-order E1 matrix elements to achieve agreement between length-form and velocity -form amplitudes.

We included here few examples of the calculated atomic data for various W ions. In particular, wavelengths, line strengths, oscillator strengths, and transition probabilities for the $\Delta n = 0$ ($3l3l' - 3l_13l_2$) transitions with rates Ar $>10^{11}$ s^{-1} in Mg-like tungsten are listed in Table 2 (Table V from [7]). The wavelengths of these transitions are in the two very small spectral regions around 22 Å and around 42 Å. A complete wavelength range of the $3l3l'-3l_13l_2$ transitions in Mg-like tungsten is much larger (from 8.2 up to 248 Å). There is a large disagreement (about 6.6%) between S_L and S_V values for transitions with very small values of Ar =10^5 s^{-1}, but good agreement (less than 0.4% difference) for transitions listed in Table 2.

We found only a few experimental measurements of energies, wavelengths and transition rates for $nl - n'l'$ transitions in Mg-, Al-, Ca-, Zn-, Ag-, and Yb-like tungsten ions. Our RMBPT results for wavelengths and transition rates Ar in Ca-like W, Al-like W, and Mg-like W ions are compared with results presented by Ralchenko et al [65] in Table 3 (Table XV from [7]). The measurements of the spectra were performed [65] at the electron beam ion trap (EBIT) at NIST. The FAC code was used to generate all relevant atomic data such as energy levels, wavelengths, and transitions probabilities [65]. Our RMBPT wavelengths for the $3s^2$ (^1S) $3p$ $^2P_{1/2} - 3p^2$ (^3P)$3s$ $^4P_{1/2}$ transition in Al-like W are in a better agreement with experimental measurement than the FAC results. The RMBPT and FAC wavelengths for the $3d_{3/2}3d_{3/2}$ $^3F_2-3d_{3/2}3d_{5/2}$ $^3F_3$ transition of Ca-like W are in a better agreement with each other than with the experimental measurement.

Table 2. Wavelengths (λ in Å), line strengths (S in a.u), oscillator strengths (f), and transition probabilities (Ar in s^{-1}) for the $\Delta n = 0$ transitions ($3l3l' - 3l_13l_2$) in Mg-like tungsten. Numbers in square brackets represent powers of 10 (Table V from [7]).

Transitions		λ	S	f	A_r	Transitions		λ	S	f	A_r
Lower	Upper	Å	a.u		s^{-1}	Lower	Upper	Å	a.u		s^{-1}
$3s3p\ ^3P_1$	$3s3d\ ^1D_2$	18.566	3.40[-3]	1.85[-2]	2.15[11]	$3s3d\ ^1D_2$	$3p3d\ ^1F_3$	23.202	2.81[-2]	7.35[-2]	6.50[11]
$3p3d\ ^3F_2$	$3d^2\ ^3F_2$	21.169	3.78[-2]	1.09[-1]	1.62[12]	$3s3d\ ^3D_3$	$3p3d\ ^3D_2$	23.253	1.34[-2]	2.50[-2]	4.31[11]
$3s3p\ ^3P_0$	$3s3d\ ^3D_1$	21.275	1.56[-2]	2.23[-1]	1.09[12]	$3s3p\ ^3P_1$	$3p^2\ ^3P_1$	23.260	1.21[-2]	5.27[-2]	6.50[11]
$3p3d\ ^1D_2$	$3d^2\ ^3P_1$	21.366	2.38[-2]	6.76[-2]	1.65[12]	$3s3d\ ^3D_1$	$3p3d\ ^3P_2$	23.272	2.73[-2]	1.19[-1]	8.76[11]
$3s3p\ ^3P_1$	$3s3d\ ^3D_2$	21.375	6.59[-2]	3.12[-1]	2.73[12]	$3s3p\ ^3P_1$	$3p^2\ ^1D_2$	23.347	1.48[-2]	6.43[-2]	4.72[11]
$3p^2\ ^1D_2$	$3p3d\ ^3D_3$	21.412	1.21[-2]	3.45[-2]	3.58[11]	$3s3d\ ^3D_2$	$3p3d\ ^3D_1$	23.372	9.88[-3]	2.57[-2]	5.22[11]
$3p3d\ ^3P_1$	$3d^2\ ^3P_0$	21.456	1.61[-2]	7.59[-2]	3.30[12]	$3s3d\ ^3D_2$	$3p3d\ ^3D_3$	23.391	1.14[-1]	2.97[-1]	2.59[12]
$3p^2\ ^3P_1$	$3p3d\ ^3D_1$	21.471	1.94[-2]	9.14[-2]	1.32[12]	$3s3d\ ^3D_3$	$3p3d\ ^3F_4$	23.779	9.67[-2]	1.77[-1]	1.62[12]
$3p^2\ ^3P_1$	$3p3d\ ^3P_0$	21.490	7.20[-3]	3.39[-2]	1.47[12]	$3s3d\ ^3D_2$	$3p3d\ ^3P_2$	23.848	8.62[-3]	2.20[-2]	2.57[11]
$3p3d\ ^1D_2$	$3d^2\ ^3P_2$	21.568	3.05[-2]	8.59[-2]	1.23[12]	$3s3p\ ^1P_1$	$3p^2\ ^3P_2$	23.895	6.20[-2]	2.63[-1]	1.84[12]
$3p^2\ ^3P_0$	$3p3d\ ^3P_1$	21.592	3.10[-2]	4.36[-1]	2.08[12]	$3s3d\ ^1D_2$	$3p3d\ ^3D_2$	24.037	4.64[-2]	1.17[-1]	1.35[12]
$3p3d\ ^3F_3$	$3d^2\ ^3F_4$	21.600	5.44[-2]	1.09[-1]	1.21[12]	$3p3d\ ^3F_4$	$3d^2\ ^1G_4$	41.475	3.74[-2]	3.04[-2]	1.18[11]
$3p3d\ ^3F_3$	$3d^2\ ^3P_2$	21.680	9.36[-3]	1.87[-2]	3.72[11]	$3p3d\ ^3D_2$	$3d^2\ ^1D_2$	41.663	5.83[-2]	8.49[-2]	3.26[11]
$3p^2\ ^1D_2$	$3p3d\ ^3P_2$	21.794	3.71[-2]	1.03[-1]	1.45[12]	$3s3p\ ^3P_2$	$3s3d\ ^3D_3$	41.775	6.26[-2]	9.10[-2]	2.48[11]
$3s3p\ ^3P_1$	$3s3d\ ^3D_1$	21.860	7.79[-3]	3.61[-2]	5.03[11]	$3p3d\ ^1P_1$	$3d^2\ ^1S_0$	42.004	2.21[-2]	5.32[-2]	6.03[11]
$3p^2\ ^3P_1$	$3p3d\ ^3P_2$	21.871	1.86[-2]	8.62[-2]	7.20[11]	$3p^2\ ^3P_2$	$3p3d\ ^1F_3$	42.364	1.16[-1]	1.66[-1]	4.41[11]
$3p3d\ ^1D_2$	$3d^2\ ^3F_3$	22.034	2.26[-2]	6.22[-2]	6.10[11]	$3p^2\ ^1D_2$	$3p3d\ ^3F_3$	42.491	3.85[-2]	5.51[-2]	1.45[11]
$3p3d\ ^3F_3$	$3d^2\ ^3F_3$	22.151	3.32[-2]	6.51[-2]	8.84[11]	$3p3d\ ^3D_1$	$3d^2\ ^3P_1$	42.807	1.40[-2]	3.31[-2]	1.20[11]
$3s3p\ ^3P_2$	$3p^2\ ^3P_2$	22.303	4.99[-2]	1.36[-1]	1.82[12]	$3p^2\ ^3P_1$	$3p3d\ ^1D_2$	43.228	4.16[-2]	9.74[-2]	2.08[11]
$3s3d\ ^3D_3$	$3p3d\ ^1F_3$	22.469	3.88[-2]	7.50[-2]	9.90[11]	$3p3d\ ^3D_3$	$3d^2\ ^3F_4$	43.237	9.04[-2]	9.07[-2]	2.52[11]
$3p3d\ ^3P_1$	$3d^2\ ^3F_2$	22.494	3.88[-2]	1.05[-1]	2.30[12]	$3p^2\ ^1S_0$	$3p3d\ ^1P_1$	43.321	2.83[-2]	1.98[-1]	2.35[11]
$3s3p\ ^3P_0$	$3p^2\ ^3P_1$	22.599	2.06[-2]	2.76[-1]	1.20[12]	$3p3d\ ^3D_1$	$3d^2\ ^3P_2$	43.624	2.71[-2]	3.78[-2]	2.21[11]
$3s3d\ ^1D_2$	$3p3d\ ^1P_1$	22.665	3.20[-2]	8.57[-2]	1.85[12]	$3p3d\ ^3P_2$	$3d^2\ ^3F_3$	43.869	5.07[-2]	7.03[-2]	1.74[11]
$3s^2\ ^1S_0$	$3s3p\ ^1P_1$	22.712	4.47[-2]	5.97[-1]	2.57[12]	$3s3p\ ^1P_1$	$3s3d\ ^1D_2$	44.735	4.47[-2]	1.01[-1]	2.02[11]
$3s3d\ ^3D_1$	$3p3d\ ^3D_1$	22.819	2.62[-2]	1.16[-1]	1.49[12]	$3p^2\ ^3P_2$	$3p3d\ ^3D_2$	45.236	2.81[-2]	3.78[-2]	1.23[11]
$3p3d\ ^3P_0$	$3d^2\ ^3P_1$	22.841	1.47[-2]	1.95[-1]	8.30[11]	$3p3d\ ^1F_3$	$3d^2\ ^1G_4$	46.167	1.30[-1]	1.22[-1]	2.98[11]
$3s3d\ ^3D_1$	$3p3d\ ^3P_0$	22.841	1.16[-2]	5.15[-2]	1.98[12]	$3p3d\ ^1P_1$	$3d^2\ ^1D_2$	46.549	2.68[-2]	3.50[-2]	1.79[11]
$3s3p\ ^1P_1$	$3p^2\ ^1S_0$	23.046	2.16[-2]	9.49[-2]	3.57[12]	$3s3p\ ^3P_1$	$3p^2\ ^3P_0$	69.665	2.14[-2]	3.11[-2]	1.28[11]

Table 3. Wavelengths (λ, Å) and transition rates Ar (s^{-1}) for Ca-like W, Al-like W, and Mg-like W ions (nuclear charge Z = 74). Comparison with theoretical (FAC) and experimental (expt.) results presented by Ralchenko *et al.* [65]. Numbers in brackets represent powers of 10 (Table XV from [7]).

			Wavelengths, λ (Å)			Transition rates A_r	
Z	Lower level	Upper level	RMBPT	expt.	FAC	RMBPT	FAC
		Ca-like tungsten					
74	$3d_{3/2}3d_{3/2}\ ^3F_2$	$3d_{3/2}3d_{5/2}\ ^3F_3$	171.57	170.78(3)	171.49	3.68[06]	3.86[06]
74	$3d_{3/2}3d_{3/2}\ ^3F_2$	$3d_{3/2}3d_{5/2}\ ^1D_2$	150.10	149.61(3)	149.80	1.80[06]	1.81[06]
		Al-like tungsten					
74	$3s^2[^1S]3p\ ^2P_{1/2}$	$3p^2[^3P]3s\ ^4P_{1/2}$	74.076	74.04(2)	73.953	3.73[10]	3.88[10]
74	$3p^2[^3P]3s\ ^4P_{1/2}$	$3s^2[^1S]3p\ ^2P_{3/2}$	63.266	63.18(3)	63.248	2.64[08]	3.05[08]
		Mg-like tungsten					
74	$3s^2\ ^1S_0$	$3s3p\ ^3P_1$	79.862	79.91(2)	79.904	1.80[10]	1.82[10]

f) <u>Relativistic many-body calculations of excitation energies and transition rates from core-excited states in silverlike ions with focus on Ag-like W [6]</u>

This work further develops the application of the relativistic many-body perturbation theory to the studies of atomic characteristics of particle-particle-hole excitations of closed-shell ions following recently performed RMBPT calculations of energies and transition rates in Na-like and in Cu-like ions. The present paper focuses on the RMBPT calculations of energies and transition rates in Ag-like ions. Energies of [Kr]$4d^9 4f^2$, [Kr]$4d^9 4f 5l$, and [Kr]$4d^9 5l 5l'$ states (with $l = s; p; d; f$) for Ag-like ions with Z = 50 -100 are evaluated to second order in relativistic many-body perturbation theory starting from a Pd-like Dirac-Fock potential ([Kr]$4d^{10}$). Second-order Coulomb and Breit-Coulomb interactions are included. Correction for the frequency-dependence of the Breit interaction is taken into account in lowest order. The Lamb shift correction to energies is also included in lowest order. Intrinsic particle-particle-hole contributions to energies are found to be 20-30% of the sum of one- and two-body contributions. Transition rates and line strengths are calculated for the $4d$ - $4f$ and $4d$ - $5l$ electric-dipole (E1) transitions in Ag-like ions with nuclear charge Z = 50 - 100. RMBPT including the Breit interaction is used to evaluate retarded E1 matrix elements in length and velocity forms. First-order RMBPT is used to obtain intermediate coupling coefficients and second-order RMBPT is used to calculate transition matrix elements. A detailed discussion of the various contributions to the dipole matrix elements and energy levels is given for silverlike tungsten (Z = 74). The transition energies included in the calculation of oscillator strengths and transition rates are from second-order RMBPT. Trends of the transition rates as functions of Z are illustrated graphically for selected transitions. Additionally, we perform calculations of energies and transition rates for Ag-like W by the Cowan code and the HULLAC code to compare with results from RMBPT code. We also constructed synthetic spectra of Ag-like W. The spectra include $4f_j\ 4f_{j'} 4d_{3/2}$ - $4f_{5/2;7/2}$ transitions which cover the spectral region from 48 to 52 Å and with additional transitions $4f_j\ 5p_{j'} 4d_{3/2}$ - $4f_{5/2;7/2}$ and $4f_j\ 5p_{j'} 4d_{5/2}$ - $4f_{5/2;7/2}$ cover the broader spectral region from 20 to 52 Å. The transitions considered in this paper form satellite lines to the brightest Pd-like lines and are of a great importance for N-shell diagnostics of heavy ions including tokamak plasmas. For example, spectrum of W in the 48- 51 Å region with strong radiation from W^{27+} to W^{29+} was observed with the TEXT tokamak at the University of Texas at Austin by Sugar *et al.* [66]. Three strong doublets of the Ag I isoelectronic sequence were identified: $4d^{10} 4f$ -

$4d^9 4f\ (^1P) 4f\ ^2D,\ ^2F,\ ^2G$. Interpolated and extrapolated wavelengths in this sequence were derived from of the difference between observed and calculated values for the transition energies. We were able to provide very accurate relativistic calculations for these transitions. All experimentally observed lines have weighted radiative probabilities $A_r \geq 10^{13}$ s^{-1}. Our RMBPT wavelengths are in excellent agreement with experimental measurements (0.1-0.7%).

2.2. Energies, radiative and autoionization rates, dielectronic satellite lines and dielectronic recombination rates *for low ionized W*

Accurate atomic data for tungsten ions are very important for correct modeling of atomic processes in tokamak plasmas such as excitation, ionization, and recombination. For example, data on recombination processes in ionized tungsten play an important role in estimation of radiation losses. We have completed relativistic calculations of low ionized W ions from Lu-like (W^{3+}) to Er-like (W^{6+}) and for Sm-like(W^{12+}) and Pm-like (W^{13+}) that cover a spectral range from 150 to 450 Å and are more relevant to the edge plasma diagnostics in tokamak. Three previously mentioned atomic codes, RMBPT, COWAN, and HULLAC have been used. Those codes allow us to check accuracy of our calculations and to produce recommendation of using these codes to calculate atomic data for specific W ions. Table 4 shows the available information from the papers. In addition, it gives ionization energies and the ground state configurations as well as the number of levels included from Refs.[66-68] . The largest number of identified levels was found to be for neutral W, for one and two times ionized W, Ta-like W^{1+} and Hf-like W^{2+}. More than hundred levels were derived for the Lu-like W^{3+} and Er-like W^{6+} . A little less (about 60) was given for Yb-like W^{4+} ion. Energies of only few levels were estimated for Tm-like W^{5+} (14) and Ho-like W^{7+} (2). In two columns we list a number of references with measurements of energy levels (experiment) and theoretical calculations of transition rates and lifetimes of levels (theory). The largest number of publications presented results for neutral W and one times ionized W, W^{1+}. Those references are listed in NIST databases [68-69]. So, we have used three above mentioned codes to fill out a gap in NIST data clearly shown by Kramida and Shirai in Ref.[66] and have calculated the relativistic data for low ionized W ions from Lu-like (W^{3+}) to Er-like (W^{6+}) and for Sm-like(W^{12+}) and Pm-like (W^{13+}) (see the last column with references to our work).

Table 4. Atomic data and number of references for neutral and low-ionized W ions.

Ion	Ground State	IP (eV) [66]	Number of refs. experiment	Number of refs. theory	Refs. this work
Neutral W	$[Pd]4f^{14}5s^25p^65d^46s^2$	7.804	11	15	
Ta-like W (W^{1+})	$[Pd]4f^{14}5s^25p^65d^46s$	16.37	8	6	
Hf-like W (W^{2+})	$[Pd]4f^{14}5s^25p^65d^4$	26.0	1	2	
Lu-like W (W^{3+})	$[Pd]4f^{14}5s^25p^65d^3$	38.2	1	0	[19]
Yb-like W (W^{4+})	$[Pd]4f^{14}5s^25p^65d^2$	51.6	2	1	[18]
Tm-like W (W^{5+})	$[Pd]4f^{14}5s^25p^65d$	64.77	2	0	[16]
Er-like W (W^{6+})	$[Pd]4f^{14}5s^25p^6$	122.01	2	0	[12]
Ho-like W (W^{7+})	$[Pd]4f^{13}5s^25p^6$	141.2	1	0	
Dy-like W (W^{8+})	$[Pd]4f^{14}5s^25p^4$	160.9	0	0	
Tb-like W (W^{9+})	$[Pd]4f^{14}5s^25p^3$	179.0	0	0	
Gd-like W (W^{10+})	$[Pd]4f^{13}5s^25p^2$	208.9	0	0	
Eu-like W (W^{11+})	$[Pd]4f^{13}5s^25p$	231.6	0	0	
Sm-like W (W^{12+})	$[Pd]4f^{14}5s^2$	258.2	0	0	[22]
Pm-like W (W^{13+})	$[Pd]4f^{13}\ 5s^2$	290.7	0	4	[23]

a) Excitation energies, radiative and autoionization rates, dielectronic satellite lines and dielectronic recombination rates for excited states of Yb-like W [18]

We have calculated a large set of atomic data relevant to the dielectronic recombination of Tm-like W^{5+} into Yb-likeW^{4+}. Energy levels, radiative transition probabilities and autoionization rates for $[Cd]4f^{14}5p^65l'nl$, $[Cd]4f^{14}5p^66l''nl$, $[Cd]4f^{14}5p^55d^2nl$, $[Cd]4f^{14}5p^55d6l''nl$, $[Cd]4f^{13}5p^65d^2nl$ and $[Cd]4f^{13}5p^65d6l''nl$ (l' = d, f, g, l'' = s, p, d, l = s, p, d, f, g and n = 5–7) states of Yb-like tungsten (W^{4+}) are calculated using the relativistic many-body perturbation theory method (RMBPT code), HULLAC code and COWAN code. Branching ratios relative to the $[Cd]4f^{14}5p^65d$, $[Cd]4f^{14}5p^66s$ and $[Cd]4f^{14}5p^66p$ thresholds in Tm-like tungsten and intensity factors are calculated for satellite lines, and dielectronic recombination (DR) rate coefficients are determined for the singly excited, as well as non-autoionizing core-excited states in Yb-like tungsten. Contributions from the autoionizing doubly excited states $[Cd]4f^{14}5p^65fnl$, $[Cd]4f^{14}5p^66l''nl$ and core-excited $[Cd]4f^{14}5p^55d^2nl$, $[Cd]4f^{14}5p^55d6l''nl$, $[Cd]4f^{13}5p^65d^2nl$, $[Cd]4f^{13}5p^65d6l''nl$ states (with *n* up to 100), which are particularly important for calculating the total DR rates, are estimated. Synthetic dielectronic satellite spectra from Yb-like W are simulated in a broad spectral range from 200 to 1400 Å. These calculations provide recommended values critically

evaluated for their accuracy for a number of W^{4+} properties useful for a variety of applications including for fusion applications.

A comparison of our results of the excitations energies for the $4f^{14}5p^{6}n'l'nl$ states obtained using the COWAN and RMBPT codes with the NIST recommended data shows 0.3–1.3% agreement for the most of levels. An excellent agreement (5–20%) between the RMBPT and the COWAN values for the $4f^{14}5p^{6}n_1l_1n_2l_2$ - $4f^{14}5p^{6}n_3l_3n_4l_4$ oscillator strengths was found. A detailed comparison of wavelengths and weighted radiative rates gA_r in Yb-like W^{4+} that include the core-excited $4f^{13}5p^{6}5d^{3}$ (L_2S_{12}) L'S'J' levels shows a reasonable agreement between the COWAN and HULLAC results. The smallest difference is found for transitions with the largest gA_r values (0.5–0.9% for wavelengths and 20–60% for transition rates). The disagreement increases to 2–3% for wavelengths and to a factor of 2–3 for the transitions with smallest gA_r values.

It was found that the autoionizing states are divided into three types of states: the 4f-core-excited $4f^{13}5p^{6}5d^{2}nl$, and $4f^{13}5p^{6}5d6l''nl$ states, the 5p-core-excited $4f^{14}5p^{5}5d^{2}nl$, $4f^{14}5p^{5}5d6l''nl$ states, and the doubly-excited $4f^{14}5p^{6}5fnl$ and $4f^{14}5p^{6}6l''nl$ states. However, the core-excited $4f^{13}5p^{6}5d^{2}6p$, $4f^{14}5p^{5}5d^{3}$, and $4f^{14}5p^{5}5d^{2}6s$ configurations are only partially autoionizing as some of the levels have energies below the ionization potential. Additionally, none of the levels of the core-excited $4f^{13}5p^{6}5d^{2}6s$ and $4f^{13}5p^{6}5d^{3}$ configurations can autoionize. Concerning the doubly-excited $4f^{14}5p^{6}6p7p$ configuration, we find that some of the levels have energies below the ionization potential. None of the levels of the singly-excited $4f^{14}5p^{6}5dnl$ configurations can autoionize, as well as of the levels of the doubly-excited $4f^{14}5p^{6}6sn_1l_1$ and $4f^{14}5p^{6}6pn_2l_2$ configurations with n_1l_1 = 6s; 5f; 5g; 6s; 6p; 6d; 6f; 7s; 7p; 7d; 7f and n_2l_2 = 6p; 5f; 6d; 7s can autoionize.

Another important results contributed in the identification of tungsten lines for modeling the ionization balance of W^{4+} and W^{5+} ions observed in spheromak plasmas. The DR in the Tm-like ionW^{5+} proceeds via electron capture into the intermediate autoionizing states of the Yb-like W^{4+} ion followed by the radiative decay to singly excited bound states:

$$W^{5+}(4f^{14}5p^{6}5d) + e \rightarrow W^{4+*}(4f^{14}5p^{6}n'l'nl+4f^{13}5p^{6}5n'l'n''l''nl+4f^{14}5p^{5}5n'l'n''l''nl) + h\nu$$
$$\downarrow \qquad\qquad \downarrow \qquad (1)$$
$$W^{5+}(4f^{14}5p^{6}(5d+6s+6p)) + e. \qquad W^{4+*}(4f^{14}5p^{6}n_1l_1n_2l_2) + h\nu$$

An alternative decay channel for the autoionizing level in equation (1) is via autoionization, and in this case the system returns to its original state $4f^{14}5p^{6}nl$ as shown by a vertical arrow in equation (1).

Assuming a Maxwellian distribution, the effective emission rate coefficient C_S^{eff} of a dielectronic satellite line can be written as

$$C_S^{eff}(j,i) = 3.3\times10^{-24}\left(\frac{I_H}{kT_e}\right)^{3/2}\frac{Q_d(j,i)}{g_0}\exp\left(-\frac{E_S(i)}{kT_e}\right) photon\, cm^3 s^{-1} \qquad (2)$$

where the intensity factor Qd(j, i) is defined as

$$Q_d(j,i) = g(i)\frac{A_r(j,i)A_a(i,i_0)}{\sum_{i'_0} A_a(i,i'_0) + \sum_k A_r(k,i)} \qquad (3)$$

and I_H is the ionization potential of hydrogen, ***j*** is the lower bound state, ***i*** is the upper autoionizing state, $\boldsymbol{i_0}$ is the initial state (i.e. the ground state $4f^{14}5p^6 5d$ of the Yb-like ion) and i_0 is the possible final state for autoionization ($4f^{14}5p^6 5d + 4f^{14}5p^6 6s + 4f^{14}5p^6 6p$ in this case).

Figure 3 shows the dielectronic satellite spectra in a broad spectral range between 210Å and 1400Å calculated for an electron temperature Te = 15 eV due to $4f^{14}5p^6 n_1 l_1 n_2 l_2 \Rightarrow [4f^{14}5p^6 n'l'nl + 4f^{13}5p^6 5n'l'n''l''nl + 4f^{14}5p^5 5n'l'n''l''nl]$ transitions (total of 2600 transitions). The limited set of transitions includes transitions with 10^{-15} cm^3 s^{-1} < C_S^{eff}(j, i) < 2.3 × 10^{-12} cm^3 s^{-1} .The effective emission rate coefficients C_S^{eff}(j, i) and Gaussian profiles with the spectral resolution R ≡ λ/Δλ = 1000 are used to synthesize these spectra.

The strongest lines shown in Fig.3a (210–250 Å) result from the $5p^6 5d6s\ ^3D_2$–$5p^5 5d^2 6s\ ^3P_2$, $5p^6 5d6s\ ^3D_3$–$5p^5 5d^2 6s\ ^3D_3$, $5p^6 5d^2\ ^3F_4$–$5p^5 5d^3\ ^3F_4$ and $5p^6 5d^2\ ^1G_4$–$5p^5 5d^3\ ^1G_4$ transitions with wavelengths λ equal to 219.02 Å, 222.27 Å, 226.33 Å, and 227.48 Å, respectively. The large number of strong lines around 400 Å –410 Å shown in Fig. 3b (250 Å –450 Å) are due to transitions between the non-autoionizing ($4f^{13}5p^6 5d^3$ + $4f^{14}5p^5 5d^3$) and the autoionizing ($4f^{13}5p^6 5d^2 5f$+ $4f^{14}5p^5 5d^2 5f$) core-excited states. The strongest lines around 276 Å –279 Å shown in Fig. 3b result from the $4f^{14}5p^6 5d6s\ ^3D_3$ − $4f^{14}5p^5 5d^2 6s\ ^5D_4$, $4f^{14}5p^6 5d6s\ ^1D_2$ − $4f^{14}5p^5 5d^2 6s\ ^3G_3$, and $4f^{14}5p^6 5d6p\ ^3F_4$ − $4f^{14}5p^5 5d^2 6p\ ^5F_5$ transitions. The values of effective emission rate coefficients C_S^{eff} for these transitions are about 200 in units of 10^{-15} cm^3 s^{-1} and are about seven times smaller than the values of C_S^{eff} coefficients in Fig.3a.

The synthetic spectrum of the DR satellite lines shown in Fig.3c (630 Å –790 Å) give another example of the contribution of transition between the core-excited states. The strongest lines around λ = 725 Å are due to the transitions between core-excited $4f^{13}5d^3$ −

$4f^{13}5d^{2}6p$ configurations. The 5d6f − 6p6f, 5d7d − 6p7d, 5d5g − 6p5g and 5d7p − 6p7p transitions contribute to the DR satellite spectrum around 650 Å –670 Å. The strongest lines around 1100 Å –1220 Å displayed in Fig. 3d (800–1400 Å) are due to transitions without excitation of the $4f^{14}5p^{6}$ core. The 6p6d − 6d2, 6s6f − 6p6f and 6p5f − 5f6d transitions occur between the non-autoionizing and autoionizing doubly excited configurations. The values of effective emission rate coefficient C_S^{eff} for these transitions are about $20\times10^{-15}cm^{3}s^{-1}$, which are the lowest among the C_S^{eff} values shown in figure 3.

b) Dielectronic recombination of Er-like tungsten [12]

Theoretical studies of dielectronic recombination, a very important process for both atomic and plasma physics, are carried out for low-ionized Er-like W. The dielectronic recombination (DR) of the Er-like ion W^{6+} proceeds via electron capture into the intermediate autoionizing states of the Tm-like ion W^{5+} followed by the radiative decay to singly-excited bound states. In particular, energy levels, radiative transition probabilities, and autoionization rates for $[Cd]4f^{14}5p^{5}5l'nl$, $[Cd]4f^{14}5p^{5}6l''nl$, $[Cd]4f^{13}5p^{6}5l'nl$, and $[Cd]4f^{13}5p^{6}6l''nl$ (l'= d,f,g, l'' = s,p,d,f,g, n = 5–7) states in Tm-like tungsten (W^{5+}) are calculated using the relativistic many-body perturbation theory and relativistic all-order single-double method as well as the Hartree-Fock-relativistic method (COWAN code). Branching ratios relative to the first threshold and intensity factors are calculated for satellite lines. DR rate coefficients are determined for the singly-excited $[Cd]4f^{14}5p^{6}nl$ (n = 5–7) and nonautoionizing doublyexcited $[Cd]4f^{14}5p^{5}5d^{2}$, $[Cd]4f^{13}5p^{6}5d^{2}$, $[Cd]4f^{13}5p^{6}6s^{2}$, $[Cd]4f^{13}5p^{6}5d6s$, and $[Cd]4f^{13}5p^{6}5d6p$ states. Also, contributions from the autoionizing doubly-excited $[Cd]4f^{14}5p^{5}5l'nl$, $[Cd]4f^{14}5p^{5}6l''nl$, $[Cd]4f^{13}5p^{6}5l'nl$, and $[Cd]4f^{13}5p^{6}6l''nl$ states (with n up to 100), which are very important for calculating total DR rates, are estimated.

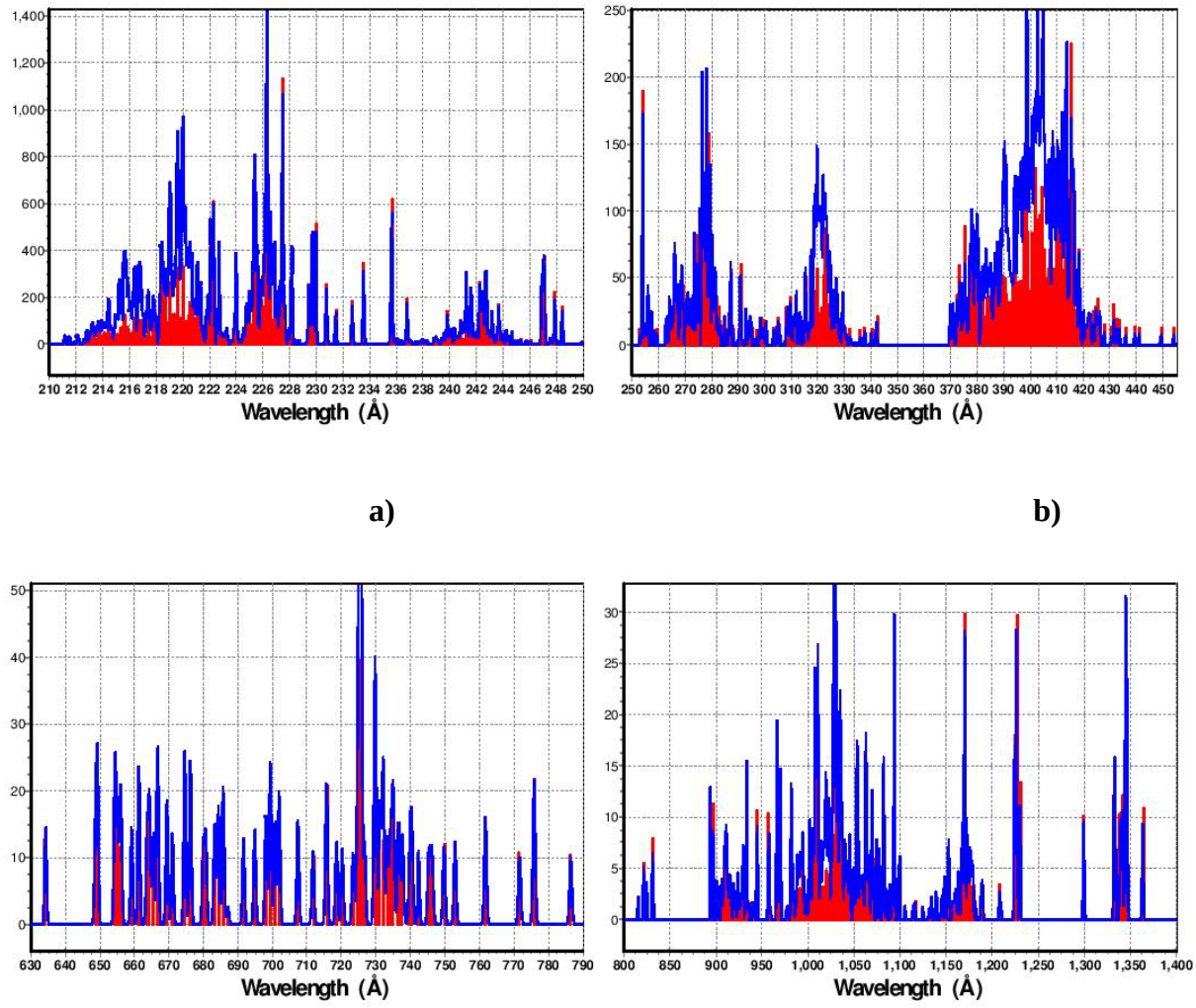

Fig. 3. Synthetic spectra (red) of dielectronic satellite lines from the W^{4+} ion at T_e = 15 eV. The scale in the ordinate is in units of 10^{-15} cm^3 s^{-1}.

Synthetic dielectronic satellite spectra from Tm-like W are simulated in a broad spectral range from 140 Å to 1200 Å. These relativistic calculations provide recommended values critically evaluated for their accuracy for a number of W^{5+} ion properties useful for a variety of applications, including for fusion applications.

The dielectronic recombination of the Er-like ionW^{6+} proceeds via electron capture into the intermediate autoionizing states of the Tm-like ion W^{5+} followed by the radiative decay to singly-excited bound states:

$$W^{6+}(4f^{14}5p^6)+e \rightarrow W^{5+}(4^{f13}5p^6nln'l'+4f^{14}5p^5nln'l') \rightarrow W^{5+}(4f^{14}5p^6nl) + h\nu$$
$$\downarrow$$
$$W^{6+}(4df^{14}5p^6) + e. \qquad (4)$$

An alternative decay channel for the autoionizing state in Eq. (4) is via autoionization. In this case, the system returns to its original state $4f^{14}5p^6$ as shown by a vertical arrow in Eq. (4).

Figure 4 shows the dielectronic satellite spectra for an electron temperature T_e=20 eV due to [$4f^{14}5p^5$5l'nl + $4f^{14}5p^5$6l''nl + $4f^{13}5p^6$5l0nl + $4f^{13}5p^6$6l00nl]) [4f145p6nl + $4f^{14}5p^5$6s^2 + $4f^{14}5p^5$5d6s +$4f^{14}5p^5$5d6p + $4f^{14}5p^5$5d^2 + $4f^{13}5p^6$5d^2 + $4f^{13}5p^6$6s^2 + $4f^{13}5p^6$5d6s + $4f^{13}5p^6$5d6p] transitions (3200 transitions in total). The limited set of transitions includes transitions with 10^{-14} cm^3 s^{-1} < C_S^{eff}(j, i) < 2.3×10^{-12} cm^3 s^{-1}. The effective emission rate coefficients C_S^{eff}(j, i) and Gaussian profiles with the spectral resolution R ≡ λ/Δλ = 400-3000 are used to synthesize these spectra. There are the doubly-excited $4f^{14}5p^5$6s^2, $4f^{14}5p^5$5d6s, and $4f^{14}5p^5$5d6p configurations only partially autoionizing. That means that some of the levels have energies below or above the ionization threshold.

The strongest lines shown in Fig.4a. result from the $4f^{14}5p^6$6d $^2D_{5/2}$- $4f^{14}5p^5$5d6d $^2F_{7/2}$ and $4f^{14}5p^6$6s $^2S_{1/2}$- $4f^{14}5p^5$5d6s $^2P_{3/2}$, $4f^{14}5p^6$6d $^2D_{3/2}$- $4f^{14}5p^5$5d6d $^2F_{5/2}$ and $4f^{14}5p^6$6s $^2S_{1/2}$- $4f^{14}5p^5$5d6s $^2P_{1/2}$ transitions with wavelengths¸ equal to 218.37Å, 218.57Å , 218.96Å, and 219.12Å, respectively. Those four lines are the satellite lines to the strong λ = 216.219Å line of the $4f^{14}5p^6$ $^1S_0$ - $4d^{14}5p^5$5d $^1P_1$ resonance transitions of Er-like tungsten.

The satellite lines to another strong line in the Er-like tungsten at λ = 261.387 Å ($4f^{14}5p^6$ $^1S_0$ – $4f^{14}5p^5$5d $^3D_1$ transition) are shown in Fig.4b. The strongest satellite lines correspond to the $4f^{14}5p^6$5f$^2F_{7/2}$ - $4f^{14}5p^5$5d5f $^4P_{5/2}$ transition (λ =262.89Å) and the $4f^{14}5p^6$5f $^2F_{5/2}$- $4f^{14}5p^5$5d5f $^2P_{3/2}$ transition (λ = 262.91 Å).The large number of strongest spectral features shown in Fig.2b result from the transitions between the non-autionizing ($4f^{13}5p^6$5d2 + $4f^{13}5p^6$5d6p + $4f^{13}5p^6$5d6s) doubly-excited states and the autionizing ($4f^{13}5p^6$5d5f + $4f^{13}5p^6$6p5f + $4f^{13}5p^6$6s5f) doubly-excited states. The wavelengths of the $4f^{13}5p^6$5d2 - $4f^{13}5p^6$5d5f, $4f^{13}5p^6$ 5d6p - $4f^{13}5p^6$6p5f, and $4f^{13}5p^6$5d6s - $4f^{13}5p^6$5f6s lines are distributed in the region of 335Å -380 Å including more than 2000 transitions. The values of effective emission rate coefficient C_S^{eff} are about 1-700 in units of $10^{-15}cm^3/s$.

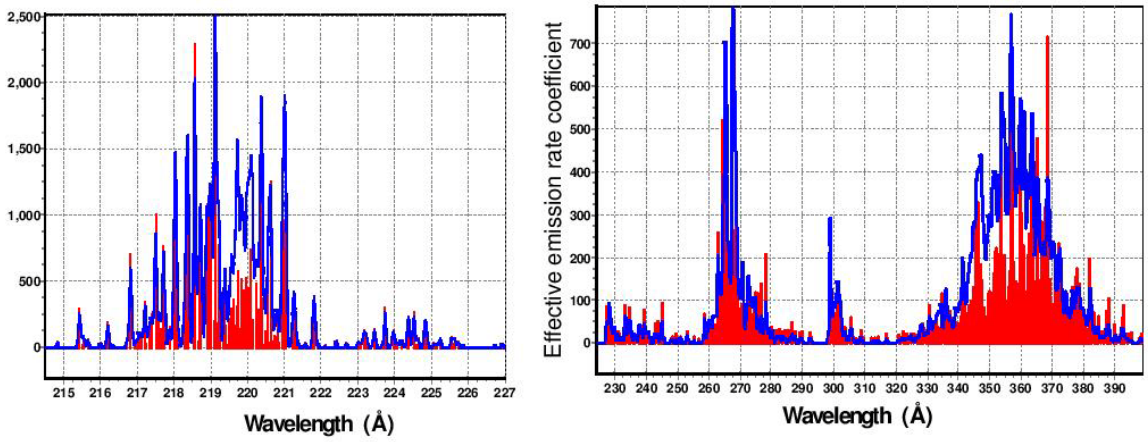

a) **b)**

Fig. 4. Synthetic spectra (red) of dielectronic satellite from the of Tm-like tungsten W^{5+} ion at T_e = 20 eV. The scale in the ordinate is in units of 10^{-15} cm^3 s^{-1}.

2.3. Spectroscopic analysis and modeling of tungsten EBIT and Z-pinch plasma experiments [2, 14, 25]

Spectral tungsten data taken on an electron beam ion trap (EBIT) at LLNL are analyzed between 3 and 8 Å for electron beam energies between 2.5 and 4.1 keV. The advantage of using charge state balancing with the experimental EBIT spectra for the identification of lines is employed and discussed. Theoretical Hebrew University Lawrence Livermore Atomic Code (HULLAC) modeling is then benchmarked against the experimental EBIT results. In particular, Co-, Ni-, Zn-, Cu-, Ga-, and Ge-like transitions were modeled independently using HULLAC to aid in charge state balancing. This model is then compared with Z-pinch plasma data collected on Zebra, the 1.6 MA pulse power generator located in the Nevada Terawatt Facility (NTF) at the University of Nevada, Reno. The model is used to calculate charge balance and average ionization levels of these experimental plasma results, with particular focus on planar tungsten arrays.

a) Theoretical Modeling

Each ion species was modeled separately using the Hebrew University Lawrence Livermore Atomic Code (HULLAC). This allowed for an extremely large number of calculated transitions. The relativistic version of HULLAC's parametric potential method, including multi-configuration interactions, was employed to calculate intermediate-coupling

detailed level energies. Existing identifications of prominent lines in experimental EBIT spectra were used to determine appropriate target states, which were used to define the ion transitions included in the model calculations. Collisional strengths and decay rates were calculated between all pairs of these defined target states for Co-, Ni-, Cu-, Zn-, Ga-, and Ge-like W ions.

b) Experimental EBIT Spectra

EBIT data were generated on the EBIT-I at Lawrence Livermore National Laboratory [70]. Six spectra were generated at specific electron beam energies E_B = 2.5, 2.7, 2.9, 3.3, 3.9, and 4.1 keV, and were recorded using an engineering model x-ray spectrometer (XRS) microcalorimeter [71]. These spectra are shown in Figures 5 and 6, with respective identifications indicated in Tables 5 and 6. Photons were filtered and detected using 14 of the 32 available independent pixels, which function as non-dispersive XRS on the microcalorimeter with a resolution of 10 eV. Since each of these experiments collected data for varying periods of time, absolute counts are not meaningful and all spectra have been normalized to emphasize relative line intensities. The small variations in wavelength registered for each of the 14 pixels were corrected and then each spectrum was calibrated by its most prominent features, using the most accurate theoretical atomic tables available [72, 73]. Given the limitations of the microcalorimeter's resolution, a small calculated error in the theoretical data that was used for calibration, and a slight margin of error in the calibration curve itself, the maximum discrepancy experimental wavelengths presented range from ±0.009 at 4.31 Å to 0.017 at 7.93 Å.

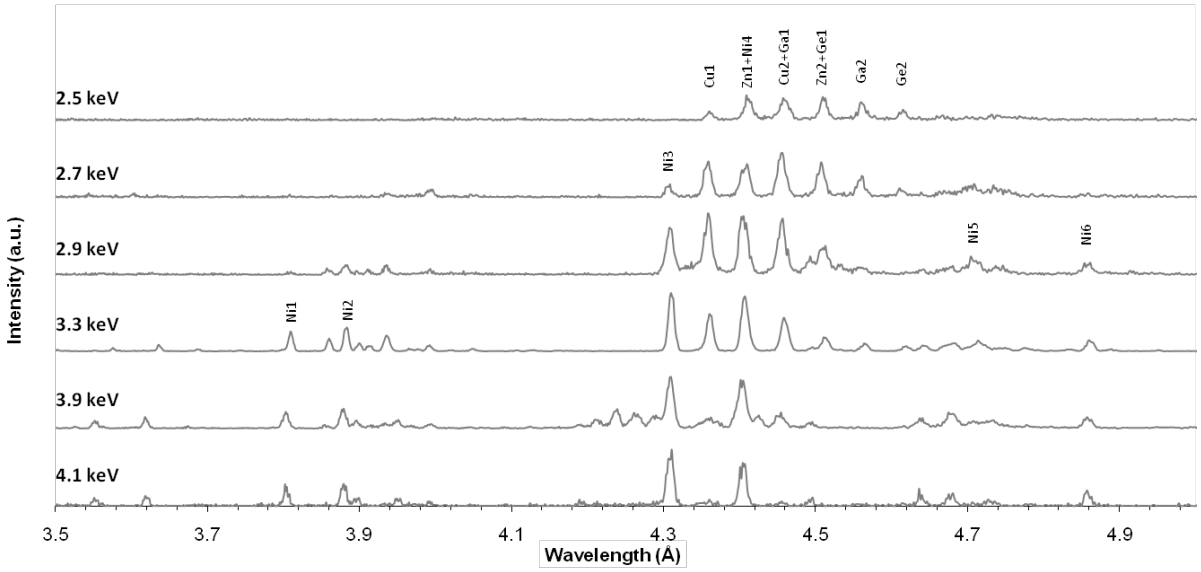

Fig. 5. *3d→5l* and *3d→6l* transitions in EBIT-I spectra at various electron beam energies, normalized within 3.5 to 5 Å on a linear scale.

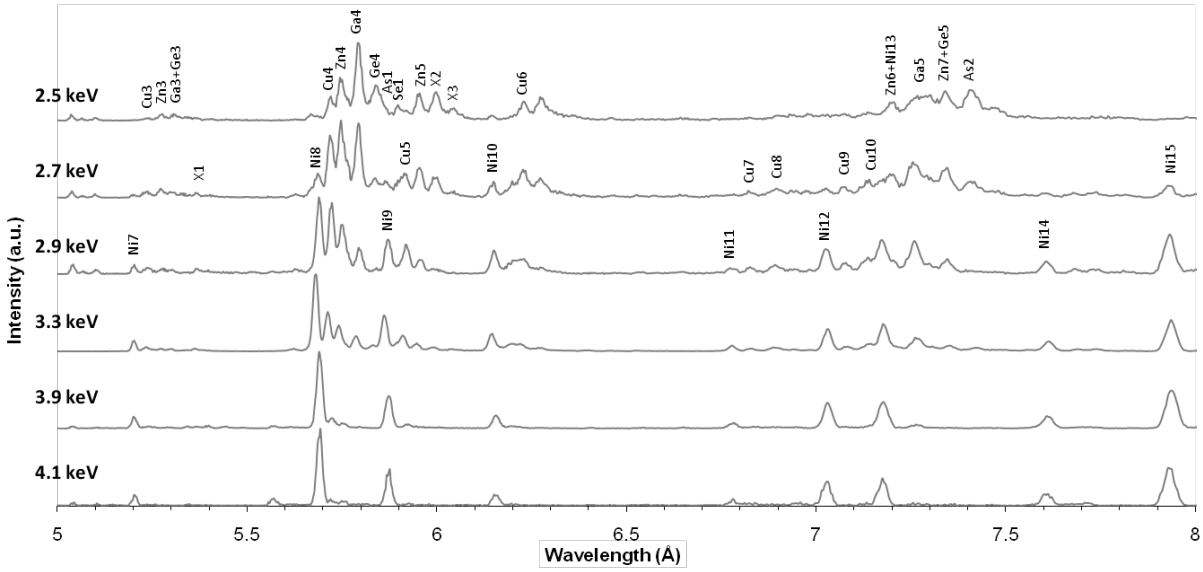

Fig. 6. *3l→4l'* transitions for EBIT-I spectra at various electron beam energies. Intensities are on a linear scale.

Table 5. 3d→5l and 3d→6l line identifications for EBIT spectra at various electron beam energies with comparisons to existing tables by Kramida and Shirai [66]. If no intensity is given, the line is blended with the one above it. Estimated uncertainties for all wavelengths listed from [66] were between ±0.002 and ±0.005 Å.

Experimental Data from EBIT-I							Kramida and Shirai [66]	
		Intensity (norm.)						
Name	λ (Å)	2.5 keV	2.7 keV	2.9 keV	3.3 keV	3.9 keV	λ (Å)	Transition
Ni1	3.802				0.041	0.020	3.803	$3d^{10}\ (^1S_0) - 3d^9 6f\ (3/2,5/2)^o_1$
Ni2	3.874			0.012	0.054	0.033	3.877	$3d^{10}\ (^1S_0) - 3d^9 6f\ (5/2,7/2)^o_1$
Ni3	4.307		0.042	0.153	0.171	0.148	4.309	$3d^{10}\ ^1S_0 - 3d^9 5f\ (3/2,5/2)^o_1$
Co1	4.309						4.309	$3d^9\ ^2D_{5/2} - 3d^8\ (^1D_2)5f\ (2,5/2)^o_{5/2}$
								$3d^9\ ^2D_{5/2} - 3d^8\ (^3F_4)5f\ (4,7/2)^o_{3/2}$
								$3d^9\ ^2D_{3/2} - 3d^8\ (^3F_3)5f\ (3,7/2)^o_{3/2}$
								$3d^9\ ^2D_{5/2} - 3d^8\ (^3F_4)5f\ (4,7/2)^o_{7/2}$
Cu1	4.355	0.030	0.116	0.199	0.082		4.359	$3d^{10}4p\ ^2P^o_{1/2} - 3d^9 4p\ (3/2,1/2)^o_1 5f\ (1,5/2)_{3/2}$
								$3d^{10}4s\ ^2S_{1/2} - 3d^9 4s\ (3/2,1/2)_1 5f\ (1,5/2)^o_{3/2}$
Zn1	4.402	0.081	0.108	0.190	0.177	0.155	4.411	$3d^{10}4s^2\ ^1S_0 - 3d^9\ (^2D_{3/2})4s^2 5f\ (3/2,5/2)^o_1$
Ni4							4.406	$3d^{10}\ ^1S_0 - 3d^9 5f\ (5/2,7/2)^o_1$
Cu2	4.455	0.072	0.145	0.182	0.081		4.457	$3d^{10}4p\ ^2P^o_{1/2} - 3d^9 4s\ (5/2,1/2)^o_2 5f\ (2,7/2)_{3/2}$
								$3d^{10}4s\ ^2S_{1/2} - 3d^9 4s\ (5/2,1/2)_2 5f\ (2,7/2)^o_{3/2}$
Ga1							4.457	$3d^{10}4s^2 4p\ ^2P^o_{1/2} - 3d^9 4s^2 4p\ (3/2,1/2)^o_1 5f\ (1,5/2)_{3/2}$
								$3d^{10}4s^2 4p\ ^2P^o_{1/2} - 3d^9 4s^2 4p\ (3/2,1/2)^o_2 5f\ (2,5/2)_{1/2}$
Zn2	4.510	0.071	0.114	0.094	0.026		4.507	$3d^{10}4s^2\ ^1S_0 - 3d^9\ (^2D_{5/2})4s^2 5f\ (5/2,7/2)^o_1$
Ge1							4.507	$3d^{10}4s^2 4p^2\ ^3P_0 - 3d^9\ (^2D_{3/2})4s^2 4p^2\ (^3P_0)\ (3/2,0)_{3/2} 5f\ (3/2,5/2)^o_1$
Ga2	4.564	0.031	0.026	0.012			4.564	$3d^{10}4s^2 4p\ ^2P^o_{1/2} - 3d^9 4s^2 4p\ (5/2,1/2)^o_3 5f\ (3,7/2)_{1/2}$
								$3d^{10}4s^2 4p\ ^2P^o_{1/2} - 3d^9 4s^2 4p\ (5/2,1/2)^o_2 5f\ (2,7/2)_{3/2}$
Ge2	4.617	0.005	0.005				4.620	$3d^{10}4s^2 4p^2\ ^3P_0 - 3d^9\ (^2D_{5/2})4s^2 4p^2\ (^3P_0)\ (5/2,0)_{5/2} 5f\ (5/2,7/2)^o_1$

Table 6. 3l→4l' line identifications for EBIT spectra at various electron beam energies with comparisons to existing tables by Kramida and Shirai [66]. (*) denotes a line identified by J. Clementson that was not included in [66]. If no intensity is given, the line is blended with the one above it. Estimated uncertainties for all wavelengths listed from [66] were between ±0.002 and ±0.005 Å.

Experimental Data from EBIT-I							Kramida and Shirai [66]	
		Intensity (norm.)						
Label	λ (Å)	2.5 keV	2.7 keV	2.9 keV	3.3 keV	3.9 keV	λ (Å)	Transition
Ni5	4.682			0.026	0.019	0.024	4.680	$3s^2 3p^6 3d^{10}\ ^1S_0 - 3s 3p^6 3d^{10} 4p\ (1/2,1/2)^o_1$
Ni6	4.860			0.029	0.036	0.021	4.857	$3p^6 3d^{10}\ ^1S_0 - 3p^5 3d^{10} 4f\ (3/2,7/2)_2$
Ni7	5.199		0.042	0.126	0.138	0.157	5.1963	$3p^6 3d^{10}\ ^1S_0 - 3p^5 3d^{10} 4d\ (3/2,5/2)^o_1$
Cu3	5.238	0.034	0.083	0.085	0.058	0.029	5.2350	$3p^6 3d^{10} 4s\ ^2S_{1/2} - 3p^5 (^2P^o_{3/2}) 3d^{10} 4s4d\ (1/2,5/2)_3\ (3/2,3)_{3/2}$
Zn3	5.280	0.045	0.083	0.071	0.026		5.2723	$3p^6 3d^{10} 4s^2\ ^1S_0 - 3p^5 (^2P^o_{3/2}) 3d^{10} 4s^2 4d\ (3/2,5/2)^o_1$
Ga3	5.304	0.085	0.078	0.052	0.032		5.302	$3p^6 3d^{10} 4s^2 4p\ ^2P^o_{1/2} - 3p^5 3d^{10} 4s^2 4p\ (3/2,1/2)_2 4d\ (1,5/2)_{3/2}$
Ge3							5.3134	$3p^6 3d^{10} 4s^2 4p^2\ ^1D_2 - 3p^5 (^2P^o_{3/2}) 3d^{10} 4s^2 4p^2 (^1D_2)\ (3/2,2)_{3/2} 4d\ (3/2,5/2)^o_2$
X1	5.369	0.034	0.045	0.048	0.022			
Ni8	5.687	0.075	0.319	1.000	1.000	1.000	5.6900	$3d^{10}\ ^1S_0 - 3d^9 4f\ (3/2,5/2)^o_1$
Cu4	5.722	0.341	0.771	0.931	0.512	0.174	5.7192	$3d^{10} 4s\ ^2S_{1/2} - 3d^9 4s\ (3/2,1/2)_1 4f\ (1,5/2)^o_{3/2}$
Zn4	5.749	0.527	1.000	0.646	0.309	0.065	5.7471	$3d^{10} 4s^2\ ^1S_0 - 3d^9 (^2D_{3/2}) (4s4p_{3/2})^o_1 4d_{3/2}\ (1,3/2)^o_{1/2}\ (3/2,1/2)^o_1$
Co2							5.7482	$3d^9\ ^2D_{5/2} - 3d^8 (^1D_2) 4f\ (2,7/2)^o_{7/2}$
Ga4	5.792	1.000	0.964	0.346	0.169		5.7951	$3d^{10} 4s^2 4p\ ^2P^o_{1/2} - 3d^9 4s^2 4p\ (3/2,1/2)^o_2 4f\ (1,5/2)_{3/2}$
Ge4	5.842	0.744	0.626	0.150			5.8378	$3d^{10} 4s^2 4p^2\ ^3P_0 - 3d^9 (^2D_{5/2}) 4s^2 4p^2 (^3P_1)\ (5/2,1)_{5/2} 4f\ (5/2,5/2)^o_1$
As1	5.853	0.335	0.170				5.8551	$3d^{10} 4s^2 4p^3\ ^2D^o_{3/2} - 3d^9 (^2D_{3/2}) 4s^2 4p^3 (^2P^o_{3/2})\ (3/2,3/2)_3 4f\ (3,5/2)_{1/2}$
Ni9	5.870		0.223	0.454	0.454	0.412	5.8665	$3d^{10}\ ^1S_0 - 3d^9 4f\ (5/2,7/2)^o_1$
Se1	5.896	0.201	0.201	0.148	0.120	0.041	5.8929	$3d^{10} 4s^2 4p^4\ ^3P_2 - 3d^9 (^2D_{5/2}) 4s^2 4p^4 (^3P_2)\ (3/2,2)_{7/2} 4f\ (7/2,5/2)^o_2$
								$3d^{10} 4s^2 4p^4\ ^3P_2 - 3d^9 (^2D_{5/2}) 4s^2 4p^4 (^3P_2)\ (3/2,2)_{3/2} 4f\ (3/2,5/2)^o_3$
								$3d^{10} 4s^2 4p^4\ ^3P_2 - 3d^9 (^2D_{5/2}) 4s^2 4p^4 (^3P_2)\ (3/2,2)_{7/2} 4f\ (7/2,5/2)^o_1$
Cu5	5.918	0.175	0.305	0.386	0.192	0.025	5.9127	$3d^{10} 4s\ ^2S_{1/2} - 3d^9 4s\ (5/2,1/2)_2 4f\ (2,7/2)^o_{3/2}$
								$3d^{10} 4s\ ^2S_{1/2} - 3d^9 4s\ (5/2,1/2)_3 4f\ (3,7/2)^o_{1/2}$
*Zn5	5.959	0.299	0.336	0.198	0.078		5.9545	$3d^{10} 4s^2\ ^1S_0 - 3d^9 (^2D_{5/2}) 4s^2 4f\ (5/2,7/2)_1$
X2	6.000	0.332	0.208	0.065	0.046	0.014		

3. Radiation from low-Z and medium-Z impurities and relevant work

3.1. EUV Spectroscopy of Low-Z Ion Plasmas for Fusion Applications [3, 9, 24]

The study of impurities is a key component of magnetic fusion research as it is directly related to plasma properties and steady-state operation. Two of the most important low-Z impurities are carbon and oxygen. The appropriate method of diagnosing these ions in

plasmas is EUV spectroscopy. In this work the results of two different sets of experiments are considered, and the spectra in a spectral region from 40 to 300 Å are analyzed. The first set of experiments was carried out at the Sustained Spheromak Physics Experiment (SSPX) at LLNL, where EUV spectra of oxygen ions were recorded. The second set of experiments was performed at the compact laser-plasma x-ray/EUV facility "Sparky" at UNR. In particular, mylar and teflon slabs were used as targets to produce carbon, oxygen, and fluorine ions of different ionization stages. Non-LTE kinetic models of O, F, and C were applied to identify the most diagnostically important spectral features of low-Z ions between 40 to 300 Å and to provide plasma parameters for both sets of experiments. For example, Fig.7 presents the modeling of the experimental oxygen spectrum (shot 16608, LLNL) which reveals plasma conditions of comparatively low electron temperature, Te = 25ev and electron density of the order of 10^{14} cm^{--3}. The most prominent features are identified as the spectral lines of the excited OVI-OV ions, namely the 150Å,173 Å ,185 Å OVI and 192.8 Å OV lines. Theory reproduces the experiment well.

We have modeled the EUV spectra recorded by a high resolution grating spectrometer LoWEUS, the Long Wavelength Extreme Ultraviolet Spectrometer, in NSTX experiments. The LoWEUS was added to NSTX in 2008 and covers the region from 60 to 400 Å with a ~160 Å field of view [9]. The major difference from SSPX EUV spectra produced at similar conditions was the dominance of Li spectral features specific for NSTX plasmas. Figure 8 presents our modeling of the experimental spectrum from NSTX shot 129294 which reveals plasma conditions of relatively low Te=25 eV for both oxygen and lithium emission. We can correlate the inferred electron temperature to a plasma radius of < 30 cm at which the oxygen radiation was produced in NSTX.

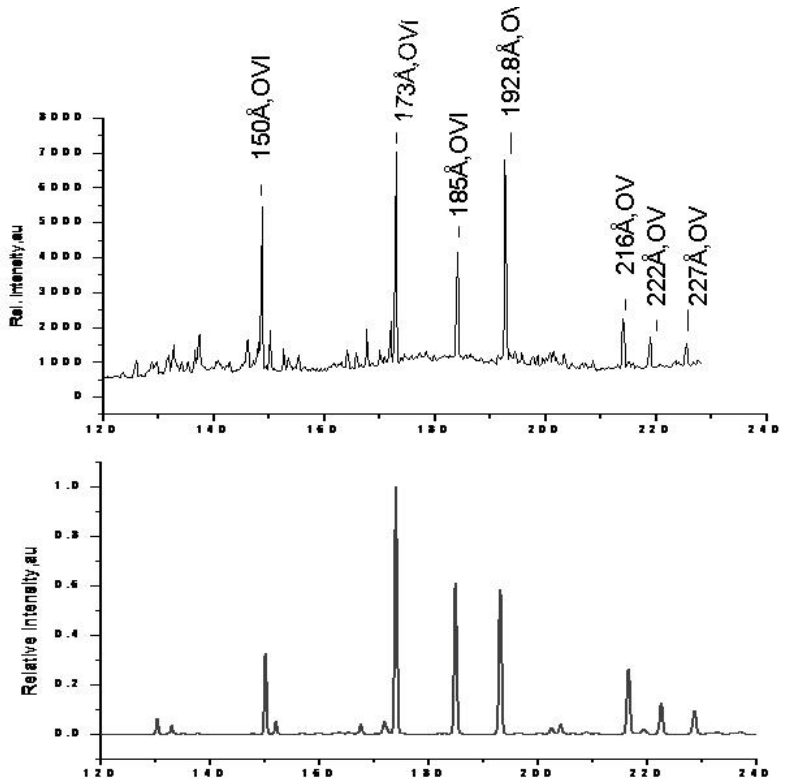

Fig. 7. Experimental spectrum from LLNL SSPX (top) fit with theoretical modeling (bottom) [3, 24].

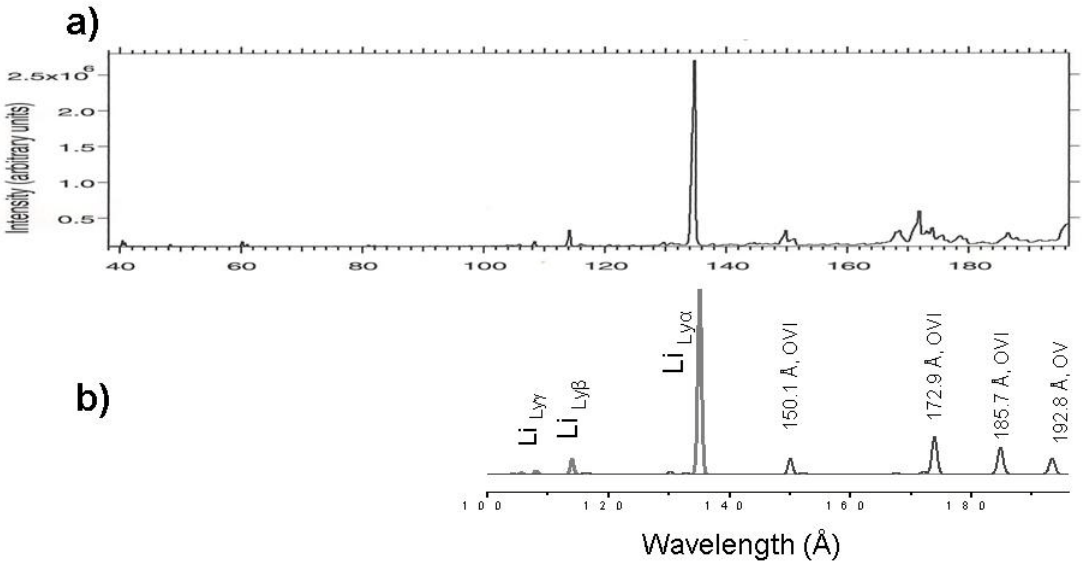

Fig. 8. The experimental spectrum produced in NSTX shot 129294 (a) fit with theoretical spectra of Li and O ions calculated at Te =25 ev and Ne=10^{14} cm^{-3} (b) [9, 24].

3.2. Extreme ultraviolet spectroscopy and modeling of Cu on the SSPX Spheromak and laser plasma "Sparky [20]

Impurities play a critical role in Spheromak research and future magnetic fusion research. They can provide information about certain plasma parameters with the use of spectroscopy, however sufficiently large quantities can cool and dilute the plasma, creating problems for magnetic confinement. Many of these impurities radiate within the extreme ultraviolet (EUV) range. In particular, the Silver Flat Field Spectrometer (SFFS) was implemented at the Sustained Spheromak Physics Experiment (SSPX) to monitor ion impurity emissions. The chamber within the SSPX was made of Cu, which makes M-shell Cu a prominent signature of impurity. To account for this, Spect3D (Prism Computational Science) was utilized to identify spectral features and to more fully understand the plasma conditions. The results of a set of SSPX experiments at LLNL in which the SFFS covered the range of 115-315 Å were analyzed in this work. A second set of experiments were carried out on the compact laser-plasma x-ray/EUV facility "Sparky" at UNR, with Cu flat targets used. The EUV spectra were recorded between 40-300 Å and compared with results on SSPX.

A major goal of this work was to identify these transitions and attain approximate parameters for plasma conditions. The most abundant transition is Cu X ($3p^5 3d^3\ ^3F_3 \rightarrow 3p^6 3d^2\ ^3F_3$) at 138.75 Å, followed by Cu XI ($3p^5 3d^2\ ^2D_{5/2} \rightarrow 3p^6 3d^1\ ^2D_{5/2}$) at 135.23 Å. Other notable transitions include Cu X ($3p^5 3d^3\ ^3D_3 \rightarrow 3p^6 3d^2\ ^3F_4$) at 132.32 Å, Cu X ($3p^5 3d^3\ ^3G_5 \rightarrow 3p^6 3d^2\ ^3F_4$) at 153.67 Å, and Cu XIII ($3p^4 3d^1\ ^2D_{5/2} \rightarrow 3p^5\ ^2P_{3/2}$) at 143.27 Å. Wavelengths were estimated both from Cowan's code and with the atomic code ATBASE run through Spect3D and compared with recommended NIST data.

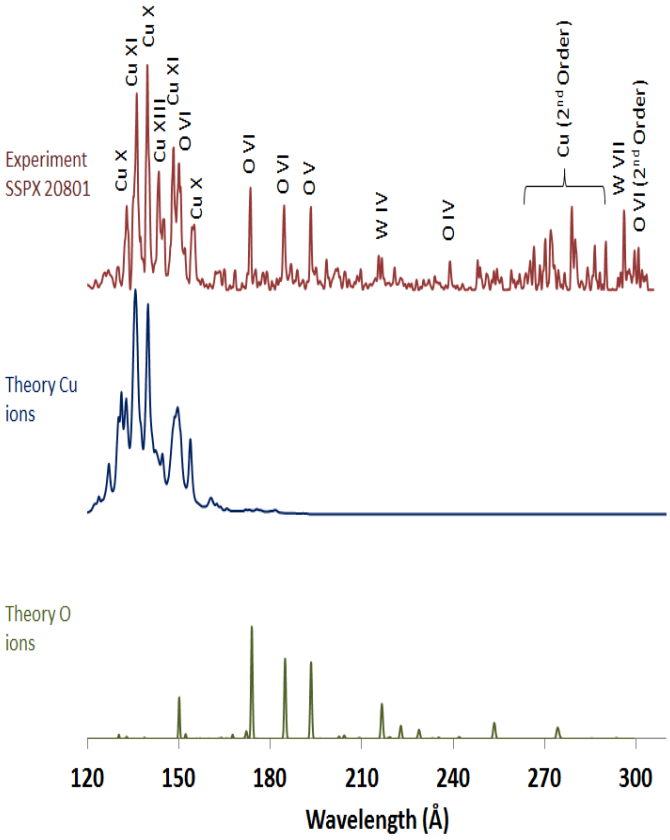

Fig. 9. Experimental spectrum of shot 20801 from SSPX at the top. Synthetic spectra calculated at $n_e = 10^{14}$ cm^{-3} for Cu spectra at $T_e = 40$ eV (in the middle) and for O spectra at $T_e = 15$ eV (at the bottom) [20].

Figure 9 displays theoretical calculations for shot 20801 on SSPX. M-shell Cu ions were calculated with Spect3D, while the O ions were calculated from SCRAM, which uses FAC[12] as the atomic code base. The plasma parameters for Cu were found to have electron temperature T_e = 40 eV and electron density $n_e = 10^{14}$ cm^{-3}. For O spectra the T_e was calculated to be slightly less at 15 eV, with the same $n_e = 10^{14}$ cm^{-3}. Similar simulations were run for the other two shots. For shot 20675, Cu spectra was modeled to have T_e = 35 eV while O spectra was modeled to have $T_e = 15$ eV. For shot 20780, Cu spectra was T_e =35 eV while O spectra was T_e = 13 eV. Electron densities were all run at $n_e = 10^{14}$ cm^{-3}.

The second set of experiments was performed on the compact laser-plasma x-ray/EUV facility “Sparky” at UNR. The EUV/soft x-ray laser plasma source operates with a 0.4 J, 3 ns, 10 Hz solid state laser. An EUV/Sliced Multilayer Grating/Glass Capillary Converter spectrometer was implemented to study the EUV spectra. A Cu slab was used as the target and shot multiple times (ranging from a few hundred to a few thousand) at different

laser intensities. Fig. 10 displays the results of a Cu slab shot approximately 220 times at maximum laser intensity. As with Ref. 10, the EUV spectra indicates a non-uniform, likely two temperature, plasma. A possible explanation for this is that the laser produces plasma with a hot inner core with a relatively cooler outer shell. The spectra is time- and spatially-integrated, so it collects the EUV radiation from different plasma conditions throughout time. Modeling from Spect3D indicates two plasma conditions, one at lower T_e = 25 eV, and one at higher T_e = 90 eV, with $n_e = 10^{19}$ cm^{-3} for both estimates.

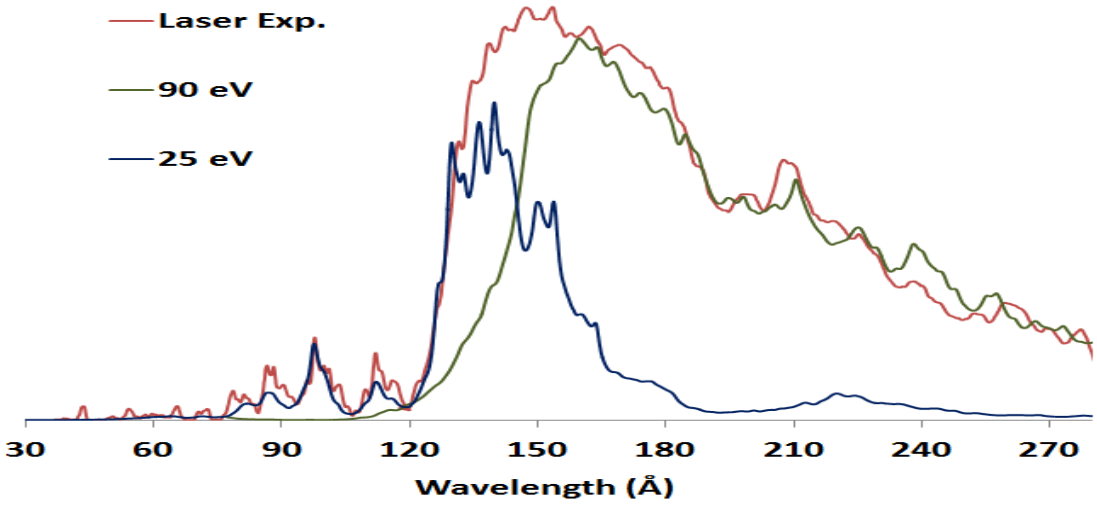

Fig. 10. Experimental spectrum of Cu EUV produced on "Sparky" with two synthetic spectrums at calculated T_e = 25 eV and 90 eV and calculated $n_e = 10^{19}$ cm^{-3} each [20].

3.3. Relativistic calculations of dielectronic recombination and satellite lines of an Ar-like Ni ion [15]

Dielectronic recombination (DR) plays an important role in understanding atomic processes and identifying spectra, including astrophysical and tokamak plasmas in particular. Because this process involves numerous singly- and doubly-excited autoionizing states, which merge with continuum states, it is challenging to calculate, and relativistic data for a lot of ions do not exist. This work focuses on relativistic calculations of dielectronic recombination in Ar-like Ni and dielectronic satellite lines in K-like Ni. Specifically, energy levels, radiative transition probabilities and autoionization rates for the $[Ne]3s^2 3p^5 3dnl$ (n = 4–7), $[Ne]3s^2 3p^5 4l'nl$ (n = 4–7), $[Ne]3s3p^6 3dnl$ (n = 4–7), $[Ne]3s3p^6 4l'nl$ (n = 4–7), $[Ne]3s^2 3p^5 5l'5l$ and $[Ne]3s3p^6 5l'5l$ states in K-like nickel (Ni^{9+}) are calculated by the Hartree–Fock relativistic method (Cowan code) and the relativistic many-body perturbation theory method (RMBPT code). In addition, these results are compared with atomic data from two more codes, HULLAC and FAC, as well as with the NIST data. DR rate coefficients are determined for the singly-excited $[Ne]3s^2 3p^6 nl$ (n = 4–7), as well as non-autoionizing doubly-excited $[Ne]3s^2 3p^5 3d^2$, $[Ne]3s^2 3p^5 3d4l$, $[Ne]3s3p^6 3d4s$ and $[Ne]3s3p^6 3d4p$ states. Contributions from the autoionizing doubly-excited states $[Ne]3s^2 3p^5 3dnl$ and $[Ne]3s3p^6 3dnl$ (with n up to 500), which are very important for calculating total DR rates, are estimated. Synthetic dielectronic satellite spectra from K-shell Ni are simulated in a broad spectral range from 45Å to 600 Å.

The DR process to a bound state of a K-like ion involves the capture of an electron by an Ar-like ion to an autoionizing state of the resulting K-like ion followed by radiative decay to a singly-excited bound state:

$$Ni^{10+}(3s^2 3p^6) + e \rightarrow Ni^{9+}(3s^2 3p^5 n_1 l_1 nl + 3s3p^6 n_1 l'_1 nl') \rightarrow N^{i9+}(3s^2 3p^6 n_1 l_2 + 3s^2 3p^5 3dnl) + h\nu$$
$$\downarrow$$
$$Ni^{10+}(3s^2 3p^6) + e. \qquad (5)$$

The ground state of Ni^{10+}, $3s^2 3p^6$, is the initial state. The $3s^2 3p^5 3dnl$ (n = 6–7), $3s3p^6 3dnl$ (n = 5–7), $3s^2 3p^5 4l'nl$ (n = 4–7), $3s3p^6 4l'nl$ (n = 4–7), $3s^2 3p^5 5l'5l$ and $3s3p^6 5l'5l$ states are indeed autoionizing states, and so are the doubly-excited $3s3p^6 3d4d$, $3s3p^6 3d4f$, $3s^2 3p^5 3d5f$ and $3s^2 3p^5 3d5g$ states. However, the doubly-excited $3s^2 3p^5 3d5s$, $3s^2 3p^5 3d5p$ and $3s^2 3p^5 3d5d$ states are only partly autoionizing. Finally, none of the levels of the doubly-excited $3s^2 3p^5 3d^2$, $3s^2 3p^5 3d4l$, $3s3p^6 3d4s$, and $3s3p^6 3d4p$ configurations can autoionize.

Figure 11 shows examples of dielectronic satellite spectra for Te = 20 eV created by $3s^23p^6nl$ – $3s^23p^53dnl$, $3s^23p^6nl$ – $3s^23p^54snl$, $3s^23p^53d^2$ – $3s^23p^53dnl$, and $3s^23p^53dnl$–$3s3p^63dnl$ transitions. In these figures, we include data for 3105 transitions. The limited set of transitions includes transitions with 10^{-14} cm^3 s^{-1} < C_S^{eff}(j, i) < 3.6 × 10^{-12} cm^3 s^{-1}. The effective emission rate coefficients C_S^{eff}(j, i) and Gaussian profiles with the spectral resolution R ≡ λ/Δλ = 700-2500 are used to synthesize these spectra.

The strongest lines shown in Fig.11a are due to the $3p^53d^2\ ^2L_J$ –$3p^53d5f\ ^2L'_{J'}$ transitions with wavelengths λ = 73.81Å – 75.49Å and relative intensities from 1040 to 3600 (in units of 10^{-15} cm^{3}s^{-1}). Those lines are situated in the region around the three lines at λ = 74.097Å, 74.266Å and 74.272Å of the $3p^63d\ ^2D_J$ –$3p^65f\ ^2F_{J'}$ transitions. The strongest lines in Fig.5b are due to the $3p^65l\ ^2L_J$ – $3p^53d5l\ ^2L'_{J'}$ transitions with wavelengths λ = 147.19Å – 148.92Å and relative intensities from 1020 to 1560 (in units of 10^{-15}cm^3 s^{-1}). Those eight lines are the satellite lines to the strongest resonance lines at λ = 148.38Å of the $3p^6\ ^1S_0$ – $3p^53d\ ^1P_1$ transition of Ar-like Ni^{10+}.

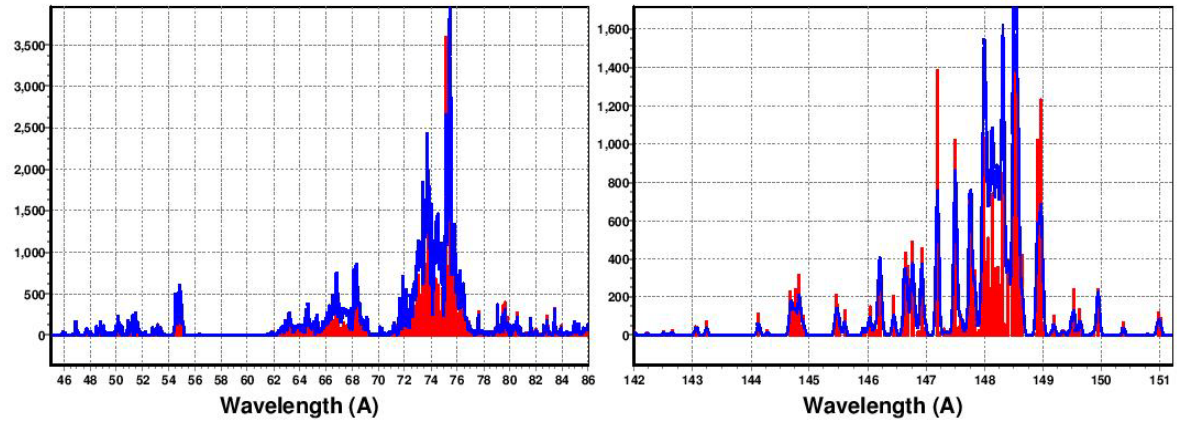

a) **b)**

Fig. 11. Synthetic spectra (red) of dielectronic satellite from the of Ar-like nickel (Ni^{10+}) ion at T_e = 20 eV. The scale in the ordinate is in units of 10^{-15} cm^3 s^{-1} [15].

The total DR rate coefficient $\alpha_d(i_0)$ is obtained by summation of the effective emission rate coefficients C_S^{eff}(j, i) (equation (6)) through all possible singly- and doubly-excited states:

$$\alpha_d(i_0) = \sum_i \sum_j C_S^{eff}(j,i) \qquad (6)$$

Here $i_0 = 3s^2 3p^6$ and **i** are all possible autoionizing doubly-excited states of Ni^{9+} with energies larger than the $3s^2 3p^6$ threshold (1812000 cm^{-1}). That includes the $3s^2 3p^5 3dnl$, $3s3p^6 3dnl$, $3s^2 3p^5 4l'nl$ and $3s3p^6 4l'nl$ doubly-excited, autoionizing states with n up to 7 (9302 levels) and $3s^2 3p^5 5l'5l$ and $3s3p^6 5l'5l$ configurations (1385 levels). The sum over **j** in equation (6) is a sum over all possible non-autoionizing states. That includes the $3s^2 3p^6 nl$ singly-excited states, as well as the non-autoionizing doubly-excited states ($3s^2 3p^5 3d^2$, $3s^2 3p^5 3d4s$, $3s^2 3p^5 3d4p$, $3s^2 3p^5 3d4d$, $3s^2 3p^5 3d4f$, $3s3p^6 3d4s$, $3s3p^6 3d4p$, $3s^2 3p^5 3d5s$, $3s^2 3p^5 3d5p$ and $3s^2 3p^5 3d5d$).

In figure 12, we illustrate the results for the total DR rate coefficient $\alpha_d(3s^2 3p^6)$. The electron temperature varies between 0.1 eV and 4.7 keV. The resulting curve labeled '4' has a peak at Te ≈ 3.0eV with a maximum value of $5.469 \times 10^{-10} cm^3 s^{-1}$ and very slowly decreases. Different contributions are shown by curves '1' through '3'. Curve '1' depicts $\alpha_d^{sing}(3s^2 3p^6)$ contribution from the singly-excited states. Curve '2' displays $\alpha_d^{doub}(3s^2 3p^6)$ contribution from non-autoionizing doubly-exited states. Curve '3' shows the combined scaled contributions $\alpha_d^{scale}(3s^2 3p^6)$ illustrated from sum for highly-excited with n=8-500. It is evident from figure 12 that the largest contribution to the total DR rate coefficient $\alpha_d(3s23p6)$ comes from curve '2' that describes the contribution from the doubly-excited non-autoionizing states. It should be noted that this large contribution from the doubly-excited non-autoionizing states was not observed previously.

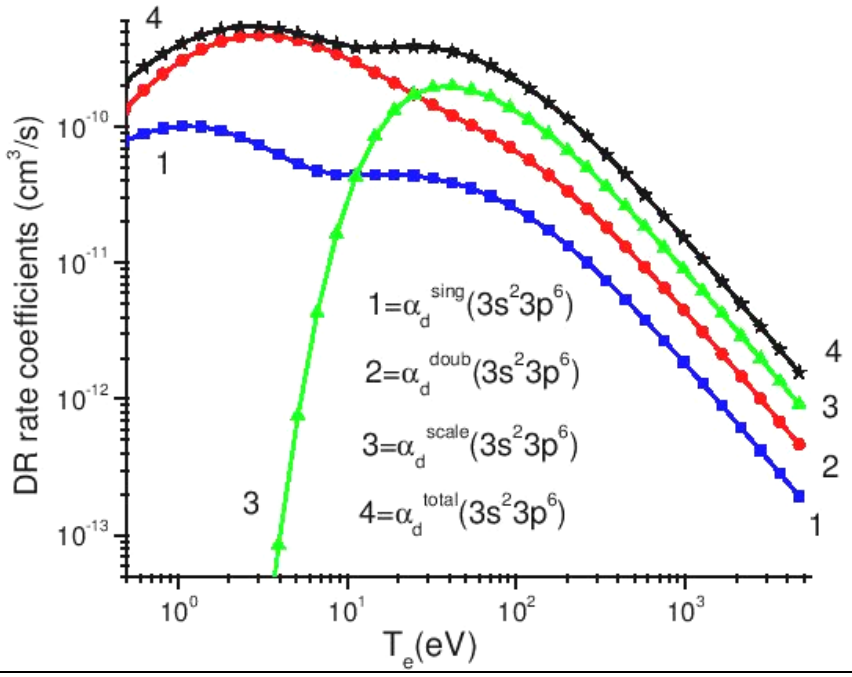

Fig. 12. Contributions from the singly-excited $\alpha_d^{sing}(3s^23p^6)$, doubly-excited non-autoionizing $\alpha_d^{doub}(3s^23p^6)$ states, and $\alpha_d^{scale}(3s^23p^6)$ high-n states to the total DR rate coefficients $\alpha_d(3s^23p^6)$ as a function of T_e in K-like nickel Ni^{9+} [15].

4. Deliverables

1. The main results of the project are highligted in the papers [1-23].
2. Four gradute students were involved in the project and two graduate students have already completed their PhD [24, 25].
3. The results were presented at 39th, 40th 41st, 42nd, 43rd and 44th Annual Meetings of the APS Division of Atomic, Molecular, and Optical Physics, 17th, 18th, and 19th Topical Conference on High Temperature Plasma Diagnostics, 35th and 36th IEEE International Conferences on Plasma Science, 16th International Conference on Atomic Processes in Plasmas, at 50th and 51st Annual Meetings of the Division of Plasma Physics, and at 10th International Colloquium on Atomic Spectra and Oscillator Strengths for Astrophysical and Laboratory Plasmas as well as at other Intrenational Conferences and Workshops [26-57].
4. The comprehensive theoretical relativistic studies of *highly ionized W* has been accomplished for a broad range of ions: Ag-like (W^{27+}), Ge-like (W^{42+}) to Co-like like (W^{47+}), Ca-like like (W^{42+}), Al-like (W^{61+}) to Ne-like like (W^{64+}), and B-like like (W^{69+}) to the highest ionized Li-like like (W^{71+}). The comparison with LLNL EBIT data has been for Ge-like (W^{42+}) to Co-like (W^{47+}). In addition, a comparison with other experimental data were made, if available.
5. The comprehensive theoretical relativistic studies of *low ionized W* has been accomplished for a broad range of ions: starting from the lowest ionized Lu-like (W^{3+}) to Er-like (W^{42+}) and Sm-like (W^{12+}) and Pm-like (W^{13+}).
6. Dielectronic recombination, an important atomic process for tokamak plasma, and dielectronic satellites lines were calculated for majority of W ions under consideration.
7. Low-Z impurities have been studied theoretically and experimentally using data from LLNL SSPX and Princeton NSTX.
8. Medium-Z impurities (Cu) have been studeid theoretically and experimentally using data from LLNL SSPX and Princeton NSTX.

5. References

5.1. Publications on the project

1. U.I. Safronova, A.S. Safronova, and P. Beiersdorfer. "*Relativistic many-body calculations of lifetimes, rated, and line strengths of multipole transitions between $3l^{-1}4l'$ states in Ni-like ions*", Physical Review A **77**, 032506 (2008)

2. G. C. Osborne, A.S. Safronova, V.L. Kantsyrev, U.I. Safronova, M.F. Yilmaz, K. Williamson, I. Shrestha, P. Beiersdorfer. "*Diagnostic of charge balance in high-temperature tungsten plasmas using LLNL EBIT*", Rev. Sci. Inst. **79**, 10E308 (2008)

3. P.G. Wilcox, A.S. Safronova, V.L. Kantsyrev, U.I. Safronova, K.M. Williamson, M.F. Yilmaz, J. Clementson, P. Beiersdorfer, K.W. Struve. "*EUV spectroscopy of low-z ion plasmas for fusion applications*", Rev. Sci. Inst. **79,** 10F543 (2008)

4. U.I. Safronova, A.S. Safronova, P. Beiersdorfer, "*Excitation energies, radiative and autoionization rates, dielectronic satellite lines, and dielectronic recombination rates for excited states of Na-like W from Ne-like W*", Atomic Data and Nuclear Data Tables **95**, 751–785 (2009)

5. U.I. Safronova, A.S. Safronova, P. Beiersdorfer, "*Excitation energies, radiative and autoionization rates, dielectronic satellite lines and dielectronic recombination rates for excited states of Mg-like W from Na-like W*", J. Phys. B: At. Mol. Opt. Phys. **42**, 165010 (17pp) (2009)

6. U.I. Safronova and A.S. Safronova, "*Relativistic many-body calculations of excitation energies and transition rates from core-excited states in silverlike ions*", Can. J. Phys. **87,** 83-94 (2009)

7. U.I. Safronova and A.S. Safronova, "*Wavelengths and transition rates for $nl - n'l'$ transitions in Be-, B-, Mg-, Al-, Ca-, Zn-, Ag-, and Yb-like tungsten ions*", J. Phys. B: At. Mol. Opt. Phys. **43,** 074026 (15pp) (2010)

8. U.I. Safronova, A.S. Safronova, W.R. Johnson, "*Relativistic many-body calculations of dielectronic satellite spectra created by autoionizing 1s2l2l' states in Li-like ions*", J. Phys. B: At. Mol. Opt. Phys., Special Issue "Spectroscopic Diagnostics of Magnetic Fusion Plasmas ", **43**, 144001 (10pp) (2010)

9. J. Lepson, P. Beiersdorfer, J. Clementson, M. F. Gu, M. Bitter, L. Roquemore, R. Kaita, P. G. Cox, A.S. Safronova. "*EUV spectroscopy on NSTX*", J. Phys. B: At. Mol. Opt. Phys., Special Issue "Spectroscopic Diagnostics of Magnetic Fusion Plasmas", **43**, 144018 (10pp) (2010)

10. A.S. Safronova,_ N. D. Ouart, J. K. Lepson, P. Beiersdorfer,3B. Stratton, M. Bitter,V. L. Kantsyrev, P. G. Cox, V. Shlyaptseva, and K. M. Williamson, ``*X-ray spectroscopy of Cu impurities on NSTX and comparison with Z-pinch plasmas''*, Rev. Sci. Inst. **81**, 10E305 (2010)

11. U.I. Safronova, A.S. Safronova, P. Beiersdorfer, and W. R. Johnson, *"Excitation energies, radiative and autoionization rates, dielectronic satellite lines and dielectronic recombination rates for excited states of Ag-likeW from Pd-like W"*, J. Phys. B: At. Mol. Opt. Phys. **44**, 035005 (15pp) (2011)

12. U.I. Safronova and A.S. Safronova, "Correlation and relativistic effects for the 4f − nl and 5p − nl *multipole transitions in Er-like tungsten*", Physical Review A **84**, 012511 (12pp) (2011)

13. U.I. Safronova, A.S. Safronova, P. Beiersdorfer, *"Dielectronic recombination and satellite line spectra of highly charged tungsten ions,* Can. J. Phys. **89**, 581-589 (2011)

14. G. C. Osborne, A.S. Safronova, V.L. Kantsyrev, U.I. Safronova, P. Beiersdorfer, K. M. Williamson, M. E.Weller, and I. Shrestha, P. " *Spectroscopic analysis and modeling of tungsten EBIT and Z-pinch plasma experiments,* Can. J. Phys. **89**, 599-608 (2011)

15. U.I.Safronova, P.G. Wilcox, A.S. Safronova, "*Relativistic calculations of dielectronic recombination and satellite lines of an Ar-like Ni ion*", J. Phys. B: At. Mol. Opt. Phys. **44** 225002 (16pp) (2011)

16. U.I. Safronova and A.S. Safronova, "*Dielectronic recombination of Er-like tungsten*", Physical Review A **85**, 032507 (15pp) (2012)

17. U.I. Safronova, A.S. Safronova, and P. Beiersdorfer, *"Relativistic atomic data for Cu-like tungsten"*, Physical Review A **86**, 042510 (2012)

18. U.I. Safronova, A.S. Safronova, and P. Beiersdorfer, *"Excitation energies, radiative and autoionization rates, dielectronic satellite lines and dielectronic recombination rates for excited states of Yb-like W"*, J. Phys. B: At. Mol. Opt. Phys. **45**, 085001 (17pp) (2012)*special recognition from the publishers

19. U.I. Safronova and A.S. Safronova, "*Correlation and relativistic effects within the trivalent Lu-like sequence''*, J. Phys. B: At. Mol. Opt. Phys. **45**, 185002 (15pp) (2012)

20. M. E. Weller,A. S. Safronova, J. Clementson, V. L. Kantsyrev, U. I. Safronova, P. Beiersdorfer, E. E. Petkov, P. G. Wilcox, and G. C. Osborne, ``*Extreme ultraviolet spectroscopy and modeling of Cu on the SSPX Spheromak and laser plasma "Sparky*", Rev. Sci. Inst. **83**, 10E101 (2012)

21. G. C. Osborne, V. L. Kantsyrev, A. S. Safronova, A. A. Esaulov, M. E. Weller, I. Shrestha, V. V. Shlyaptseva, and N. D. Ouart, ``*X-ray absorption spectroscopy of aluminum z-pinch plasma with tungsten backlighter planar wire array source''* Rev. Sci. Inst. **83**, 10E103 (2012)

22. U.I. Safronova, A.S. Safronova, P. Beiersdorfer, "*Relativistic many-body calculations of excitation energies, oscillator strengths, transitions rates, and lifetimes in samariumlike ions*", Physical Review A **87**, 032508 (pp14) (2013)

23. U.I. Safronova, A.S. Safronova, P. Beiersdorfer, "*Contribution of the 4f-core-excited states in determination of atomic properties in the promethium isoelectronic sequence*", Physical Review A **88**, 032512 (pp11) (2013).

5.2. PhD Dissertations

24. P.G. Wilcox, "*Low- and mid-Z EUV spectroscopy of high temperature plasmas"*, PhD Dissertation, University of Nevada, Reno, 2011.

25. G.C. Osborne, *"An Investigation of Tungsten-Based Z-Pinch Planar Wire Array and Benchmarking Experiments"*, PhD Dissertation, University of Nevada, Reno, 2012.

5.3. Presentations on the project

26. G. C. Osborne, A.S. Safronova, V.L. Kantsyrev, U.I. Safronova, M.F. Yilmaz, K. Williamson, I. Shrestha, P. Beiersdorfer. " *Diagnostic of charge balance in high-temperature tungsten plasmas using LLNL EBIT*", 17th Topical Conference on High Temperature Plasma Diagnostics, Albuquerque, NM, May 11-15 (2008)

27. P.G. Wilcox, A.S. Safronova, V.L. Kantsyrev, U.I. Safronova, K.M. Williamson, M.F. Yilmaz, J. Clementson, P. Beiersdorfer, K.W. Struve. "*EUV spectroscopy of low-z ion plasmas for fusion applications*", 17th Topical Conference on High Temperature Plasma Diagnostics, Albuquerque, NM, May 11-15 (2008)

28. U.I. Safronova, A.S. Safronova, P. Beiersdorfer. "*Overview of recent results on lifetimes, rates, and line strengths of multipole transitions from $3l^{-1}4l'$ states in Ni-like ions*", 39th Annual Meeting of the APS Division of Atomic, Molecular, and Optical Physics, State College , PA (May 27-31, 2008)

29. A.S. Safronova, U.I. Safronova, P. Beiersdorfer. "*Excitation energies, radiative and autoionization rates, dielectronic satellite lines, and dielectronic recombination rates for excited states of Na-like W from Ne-like W*", 39th Annual Meeting of the APS Division of Atomic, Molecular, and Optical Physics, State College , PA (May 27-31, 2008)

30. A.S. Safronova, U.I. Safronova, V.L. Kantsyrev, G.C. Osborne, N.D. Ouart, K.M. Williamson,I. Shrestha, P. Beiersdorfer, "*Theoretical Development of X-Ray Diagnostics of Tungsten Ions for Fusion and HEDP Applications*", The 35th IEEE International Conference on Plasma Science, p. 87, Karlsruhe, Germany, June 15-19 (2008)

31. G.C. Osborne, A.S. Safronova, U.I. Safronova, V.L. Kantsyrev, K.M. Williamson, I. Shrestha, P. Beiersdorfer, "*Charge balancing and identification of prominent spectral*

features of M-shell W plasmas", 50th Annual Meeting of the Division of Plasma Physics, Dallas, TX, Nov. 17-21, 2008

32. P.G. Wilcox, A.S. Safronova, V.L. Kantsyrev, U.I. Safronova, K.M. Williamson, M.E. Weller, J. Clementson, P. Beiersdorfer, K.W. Struve, *"Analysis of EUV Oxygen Spectra from LLNL SSPX and UNR Laser Plasma Source of "Sparky"*, 50th Annual Meeting of the Division of Plasma Physics, Dallas, TX, Nov. 17-21, 2008

33. U.I. Safronova, A.S. Safronova, P. Beiersdorfer, *"Atomic data for dielectronic satellite lines and dielectronic recombination into Na-like W^{63+}"*, 16th International Conference on Atomic Processes in Plasmas, Monterey, CA (March 22-26, 2009)

34. P.G. Wilcox, A.S. Safronova, V.L. Kantsyrev, A.A. Esaulov, U.I. Safronova, K.M. Williamson, G.C. Osborne, M.E. Weller, J. Clementson, P. Beiersdorfer, J. Lepson. *"Study of Low-Z EUV Spectra from Laboratory Plasma and EBIT Experiments"*, 40th Annual Meeting of the APS Division of Atomic, Molecular, and Optical Physics, Charlottesville, VA (May 19-23, 2009)

35. U.I. Safronova, A.S. Safronova, P. Beiersdorfer. *"Excitation energies, radiative and autoionization rates, dielectronic satellite lines, and dielectronic recombination rates for excited states of Mg-like W from Na-like W"*, 40th Annual Meeting of the APS Division of Atomic, Molecular, and Optical Physics, Charlottesville, VA (May 19-23, 2009)

36. A.S. Safronova, U.I. Safronova, *"Wavelengths and transition rates for nl-n'l' transitions in Na-, Mg-, Al-, K-, Ca-, Zn-, Cd-, and Yb-like tungsten ions"*, 40th Annual Meeting of the APS Division of Atomic, Molecular, and Optical Physics, Charlottesville, VA (May 19-23, 2009)

37. G.C. Osborne, V.L. Kantsyrev, A.S. Safronova, A.A. Esaulov, M.F. Yilmaz, K.M. Williamson, I. Shrestha, *"Comparative Analysis of Implosions of Tungsten Single and Double Planar Wire Arrays produced on 1-MA Generator at UNR"*, The 36th IEEE International Conference on Plasma Science, San Diego, CA (May 31-June 5, 2009)

38. G.C. Osborne, A.S. Safronova, V. L. Kantsyrev, U.I. Safronova, P. Beiersdorfer, K. M. Williamson, M. E. Weller, I. Shrestha, "*X-ray spectroscopic analysis of multiply-charged tungsten ions benchmarked with LLNL EBIT data and compared with Z-pinch experiments*", 10th International Colloquium on Atomic Spectra and Oscillator Strengths for Astrophysical and Laboratory Plasmas, August 3 - 7, 2010, Berkeley, CA

39. P. G. Cox, A.S. Safronova, V. L. Kantsyrev, U.I. Safronova, K. M. Williamson, N.D. Ouart, M. E. Weller, G. C. Osborne, J. K. Lepson, P. Beiersdorfer, "*Analysis of nickel and low-Z impurity EUV and SXR radiation from NSTX and comparison with laser plasma spectra*", 10th International Colloquium on Atomic Spectra and Oscillator Strengths for Astrophysical and Laboratory Plasmas, August 3 - 7, 2010, Berkeley, CA

40. U.I. Safronova, A. S. Safronova, P. Beiersdorfer, W. R. Johnson, "*Dielectronic recombination and satellite line spectra of highly-charged tungsten ions*", 10th International Colloquium on Atomic Spectra and Oscillator Strengths for Astrophysical and Laboratory Plasmas, August 3 - 7, 2010, Berkeley, CA

41. G.C. Osborne, A.S. Safronova, V. L. Kantsyrev, U.I. Safronova, P. Beiersdorfer, K. M. Williamson, M. E. Weller, I. Shrestha, "*X-ray spectroscopic analysis of multiply-charged tungsten ions Benchmarked with LLNL EBIT data and compared with Z-pinch plasma experiments*", NNSA/DOE Review, NTF/UNR, October 27, 2010

42. P.G. Cox, A.S. Safronova, V. L. Kantsyrev, U.I. Safronova, K. M. Williamson, N.D. Ouart, M. E. Weller, G. C. Osborne, J. K. Lepson, P. Beiersdorfer, "*Analysis of nickel and low-Z impurity EUV/SXR radiation from NSTX and comparison with laser plasma spectra*", NNSA/DOE Review, NTF/UNR, October 27, 2010

43. P. G. Cox, A.S. Safronova, V. L. Kantsyrev, A.A. Esaulov, U.I. Safronova, K. M. Williamson, M. E. Weller, J. Lepson, P. Beiersdorfer, "*Modeling of low-Z plasma spectroscopy results from NSTX and compact "Sparky" plasma facilities*", The 41st Annual Meeting of the Division of Atomic Molecular and Optical Physics American Physical Society, May 25-29, 2010, Houston, Texas.

44. U.I. Safronova and A. S. Safronova, W. R. Johnson, "*Dielectronic satellite spectra of Li-like ions calculated using relativistic many-body theory for spectroscopy of high-Z multiply-charged ion plasmas*", The 41st Annual Meeting of the Division of Atomic Molecular and Optical Physics American Physical Society, May 25-29, 2010, Houston, Texas.

45. A.S. Safronova, N.D. Ouart, J.K. Lepson, P. Beiersdorfer, B. Stratton, M. Bitter, V. L. Kantsyrev, V. Shlyaptseva, P.G. Cox, K.M. Williamson, *"X-ray spectroscopy of Cu impurities on NSTX and comparison with Z-pinch plasmas"*, 18th Topical Conference High-Tempearture Plasma Diagnostics, Wilwood, NJ, May 16-20, 2010

46. W. R. Johnson, U.I. Safronova, and A.S. Safronova, "*Relativistic dielectronic recombination data for low-ionized W''*, 42nd Annual Meeting of the APS Division of Atomic, Molecular, and Optical Physics, Atlanta, Georgia (June 13-17, 2011)

47. P. G. Cox, .U.I. Safronova, and A.S. Safronova, *"Dielectronic recombination of Ar-like Ni ion and satellite lines of K-like Ni ion'', ,* 42nd Annual Meeting of the APS Division of Atomic, Molecular, and Optical Physics, Atlanta, Georgia (June 13-17, 2011).

48. G.C. Osborne, V.L. Kantsyrev, A.S. Safronova, A.A. Esaulov, U.I. Safronova, I. Shrestha, V.V. Shlyaptseva, K.M. Williamson, M.E Weller, ``*Radiative Properties and Implosion Characteristics of Planar Tungsten Wire Arrays on the Zebra Generator*, Radiation from High Energy Density Plasmas International Workshop, Nevada, Reno (March 15-18).

49. U.I. Safronova, A. Stafford, A.S. Safronova, ``*New Calculations of Dielectronic Satellite Spectra of Mg ions''*, Radiation from High Energy Density Plasmas International Workshop, Nevada, Reno (March 15-18).

50. P. Beiersdorfer, U.I. Safronova, and A.S. Safronova, *"Excitation energies, radiative and autoionization rates, dielectronic satellite lines and dielectronic recombination rates for excited states of Yb-like W"*, 43nd Annual Meeting of the APS Division of Atomic, Molecular, and Optical Physics, Anaheim, California (June 6-8, 2012).

51. U.I. Safronova, and A.S. Safronova, ``*Relativistic many-body calculations of energies in a broad range of Lu-like ions from W^{3+} to Fm^{29+}*", 43nd Annual Meeting of the APS Division of Atomic, Molecular, and Optical Physics, Anaheim, California (June 6-8, 2012).

52. A.S. Safronova, *"Spectroscopy of Z-pinch plasmas: how atomic and plasma physics merge and unfold new applications"*, 43nd Annual Meeting of the APS Division of Atomic, Molecular, and Optical Physics, Anaheim, California (June 6-8, 2012).Invited.

53. U.I. Safronova, A.S. Safronova, and P. Beiersdorfer, ``*Dielectronic recombination of low-ionized tungsten ions''*, The 23rd International Conference on Atomic Physics ICAP 2012, 23-27 July 2012, Ecole Polytechnique Palaiseau, France.

54. U.I. Safronova and A.S. Safronova, *"Correlation and relativistic effects for the 4f - nl and 5p- nl multipole transitionsin Er-like''*, The 23rd International Conference on Atomic Physics ICAP 2012, 23-27 July 2012 Ecole Polytechnique Palaisea, France.

55. M. E. Weller,A. S. Safronova, J. Clementson, V. L. Kantsyrev, U. I. Safronova, P. Beiersdorfer, E. E. Petkov, P. G. Wilcox, and G. C. Osborne, ``*EUV Spectroscopy and Modeling of Cu on the SSPX Spheromak''* 19th Topical Conference High-Temperature Plasma Diagnostics, Monterey, CA, May 6-10, 2012 .

56. G. C. Osborne, V. L. Kantsyrev, A. S. Safronova, A. A. Esaulov, M. E. Weller, I. Shrestha, V. V. Shlyaptseva, and N. D. Ouart, ``*X-ray absorption spectroscopy of aluminum z-pinch plasma with tungsten backlighter planar wire array source''* 19th Topical Conference High-Temperature Plasma Diagnostics, Monterey, CA, May 6-10, 2012 .

57. U.I. Safronova and A. S. Safronova, P.Beiersdorfer, *"Relativistic many-body calculations of excitation energies, oscillator strengths, transition rates, and lifetimes in samarium like ions"*, 2013 Joint Meeting of the APS Division of Atomic, Molecular & Optical Physics and the CAP Division of Atomic, Molecular & Optical Physics, Canada, Quebec City, Canada, June 3-7, 2013.

5.4. Additional references

58. B.C. Stratton *et al "Passive Spectroscopic Diagnostics for Magnetically Confined Fusion Plasmas"*, Fusion Sci. Tech. 53, 431 (2008).

59. T. Sugie, A. Costley, A. Malaquias, C. Walker. "*Spectroscopic diagnostics for ITER*". J. Plasma Fusion Res. **79**, 1051-1061 (2003).

60. P. Beiersdorfer *et al*, Rev. Sci. Instr. **77**, 10F306 (2006) P. Beiersdorfer, M.Bitter, L. Roquemore, J.K. Lepson, M. F. Gu. "*Grazing-incidence spectrometer for soft x-ray and extreme ultraviolet spectroscopy on the national spherical torus experiment*'', Rev. Sci. Instr. **77**, 10F306 (2006)

61. R.D. Cowan, "*The Theory of Atomic Structure and Spectra"*, University of California Press, Berkeley, 1981.

62. A. Bar-Shalom, M. Klapish, J. Oreg. "*HULLAC, an integrated computer package for atomic processes in plasmas*". JQSRT **71**, 169 (2001).

63. M.F. Gu. "*Flexible Atomic Code*". Canadian Journal of Physics **86**(5), 675-689 (2008).

64. U. Feldman, J.F. Seely, E. Landi ,Yu. Ralchenko. "*Bright EUV lines emitted by highly ionized tungsten ions as diagnostic indicators of the tungsten transport in ITER core plasmas (Te > 7 keV)"*, Nucl. Fusion **48,** 045004 (2008)

65. Y. Ralchenko, I.N. Draganic, J.N. Tan, J.D. Gillaspy, J.M. Pomeroy, J M, Reader, U. Feldman, G.E. Holland. "*EUV spectra of highly-charged ions* W^{54+} - W^{63+} *relevant to ITER diagnostics"*, J. Phys. B: At. Mol. Opt. Phys. **41** 021003 (2008)

66. A.E. Kramida, T. Shirai. "*Energy levels and spectral lines of tungsten, W III through W LXXIV*", Atomic Data and Nuclear Data Tables 95, 305–474 (2009)

67. A. E. Kramida and T. Shirai. "*Compilation of Wavelengths, Energy Levels, and Transition Probabilities for W I and W II"*, J. Phys. Chem. Ref. Data, **35**, 423 (2006).

68. A. E. Kramida and J. Reader. *Ionization energies of tungsten ions:* W^{2+} *through* W^{71+}", At. Data and Nucl. Data Tables **92**, 457 (2006).

69. Yu. Ralchenko, F.-C. Jou, D.E. Kelleher, A.E. Kramida, A. Musgrove, J. Reader, W.L. Wiese, K. Olsen. NIST Atomic Spectra Database, version 3.0.2, 2005.Available at: <http://physics.nist.gov/asd3> (2006, January 4). NIST

70. P. Beiersdorfer, "*Brief history of EBIT*", Can. J. Phys. 86, 1-10 (2008).

71. F.S. Porter, M.D. Audley, P. Beiersdorfer, K.R. Kevin, R.P. Brekosky, G.V. Brown, K.C. Gendreau, J.D. Gygax, S.M. Kahn, et al. Proc. SPIE, 4140, 407 (2000).

72. U.I. Safronova, A.S. Safronova, S.M. Hamasha, and P. Beiersdorfer. At. Data Nucl. Data Tables, 92, 47 (2006).

73. P. Neill, C. Harris, A.S. Safronova, S. Hamasha, S. Hansen, U.J. Safronova, and P. Beiersdorfer. Can. J. Phys. 82, 931 (2004).